



# Timing and climatic drivers for glaciation across semi-arid western Himalayan–Tibetan orogen



Jason M. Dortch<sup>a,\*</sup>, Lewis A. Owen<sup>b</sup>, Marc W. Caffee<sup>c</sup>

<sup>a</sup> School of Environment and Development, The University of Manchester, Manchester M0 1QD, UK

<sup>b</sup> Department of Geology, University of Cincinnati, Cincinnati, OH 45221, USA

<sup>c</sup> Department of Physics/PRIME Laboratory, Purdue University, West Lafayette, IN 47906, USA

## ARTICLE INFO

### Article history:

Received 21 January 2013

Received in revised form

17 July 2013

Accepted 20 July 2013

Available online

### Keywords:

Cosmogenic radionuclide dating

Himalaya

Tibet

Glaciation

Moraine

Chronology

Gaussian

## ABSTRACT

Mapping and forty-seven new <sup>10</sup>Be ages help define the timing of glaciation in the Ladakh and Pangong Ranges in Northwest India. Five new local glacial stages are defined for the Ladakh Range. From oldest to youngest these include: the Ladakh-4 glacial stage at  $81 \pm 20$  ka; the Ladakh-3 glacial stage (not dated); the Ladakh-2 glacial stage at  $22 \pm 3$  ka; the Ladakh-1 glacial stage (not dated); and the Ladakh Cirque glacial stage at  $1.8 \pm 0.4$  ka. Three local glacial stages are defined for the Pangong Range, which include: the Pangong-2 glacial stage at  $85 \pm 15$  ka; the Pangong-1 glacial stage at  $40 \pm 3$  ka; and the Pangong Cirque glacial stage at  $0.4 \pm 0.3$  ka. The new <sup>10</sup>Be ages are combined with 645 recalculated <sup>10</sup>Be ages from previous studies to develop the first regional framework of glaciation across the dryland regions of the Greater Himalaya, Transhimalaya, Pamir and Tian Shan at the western end of the Himalayan–Tibetan orogen. Nineteen regional glacial stages are recognized that are termed semi-arid western Himalayan–Tibetan stages (SWHTS). These include: SWHTS 9 at  $311 \pm 32$  ka; SWHTS 7 at  $234 \pm 44$  ka [tentative]; SWHTS 6 at  $146 \pm 18$  ka; SWHTS 5E at  $121 \pm 11$  ka; SWHTS 5A at  $80 \pm 5$  ka; SWHTS 5A- at  $72 \pm 8$  ka; SWHTS 4 at  $61 \pm 5$  ka; SWHTS 3 at  $46 \pm 4$  ka; SWHTS 2F at  $30 \pm 3$  ka; SWHTS 2E at  $20 \pm 2$  ka; SWHTS 2D at  $16.9 \pm 0.7$  ka; SWHTS 2C at  $14.9 \pm 0.8$  ka; SWHTS 2B at  $13.9 \pm 0.5$  ka; SWHTS 2A at  $12.2 \pm 0.8$  ka; SWHTS 1E at  $8.8 \pm 0.3$  ka [tentative]; SWHTS 1D at  $6.9 \pm 0.2$  ka [tentative]; SWHTS 1C at  $3.8 \pm 0.6$  ka; SWHTS 1B at  $1.7 \pm 0.2$  ka; and SWHTS 1A at  $0.4 \pm 0.1$  ka. Regional glacial stages older than 21 ka are broadly correlated with strong monsoons. SWHTS that are 21 ka or younger, have smaller uncertainties and broadly correlate with global ice volume given by marine Oxygen Isotope Stages, and northern hemisphere climatic events (Oldest Dryas, Older Dryas, Younger Dryas, Roman Humid Period, and Little Ice Age).

Crown Copyright © 2013 Published by Elsevier Ltd. All rights reserved.

## 1. Introduction

Glaciation in high mountains, such as the Himalayan–Tibetan orogen, exerts a strong control on the development of topography (Brozović et al., 1997), influences tectonics (Zeitler et al., 2001; Willett, 2010) and climate (Molnar and England, 1990), can condition mountain systems and focus erosion (Norton et al., 2010), and may limit fluvial incision (Korup and Montgomery, 2008). Defining the timing and extent of glaciation both locally and regionally is a critical first step toward understanding landscape evolution and paleoenvironmental change in glaciated mountains. As a move towards developing a glacial framework within one of the world's most active and impressive orogens, the Himalayan–Tibetan orogen, we construct a glacial chronostratigraphy, defined using <sup>10</sup>Be

terrestrial cosmogenic nuclides, for its western end. This includes 47 new <sup>10</sup>Be ages for the Ladakh region in northern India and reassessment of previous <sup>10</sup>Be studies across this part of the orogen.

Numerous studies, including cosmogenic nuclides and luminescence, show the complexity of the glacial records in the Himalayan–Tibetan orogen (Phillips et al., 2000; Richards et al., 2000a,b; Taylor and Mitchell, 2000; Owen et al., 2001, 2002, 2003, 2006, 2008, 2012; Seong et al., 2007, 2009a,b,c; Dortch et al., 2010a; Hedrick et al., 2011). These studies indicate that in some regions, particularly monsoon-influenced areas, Quaternary glaciation was extensive, while in others, primarily semi-arid areas, glaciation was relatively restricted over time (Owen et al., 2005, 2008 and references therein). In the monsoon-influenced regions extensive Quaternary glacial advances, high precipitation, and the associated runoff have conspired to destroy much of the evidence for past glaciation. In contrast, in the semi-arid regions of the Himalayan–Tibetan orogen, such as the Transhimalaya, old glacial landforms and well-preserved multiple sets of moraines are common (Owen

\* Corresponding author.

E-mail address: [jason.dortch@manchester.ac.uk](mailto:jason.dortch@manchester.ac.uk) (J.M. Dortch).

et al., 2005, 2008 and references therein). Semi-arid regions have a greater potential for preserving more complete glacial chronologic records. We accordingly focus on the semi-arid regions at the western end of the Himalayan–Tibetan orogen; directing our efforts on several valleys in the Ladakh and Pangong ranges of Ladakh, Northern India.

In addition to the impressive successions of moraines in Ladakh, the region also contains some of the oldest preserved moraines in the Himalayan–Tibetan orogen (Owen et al., 2006). Ladakh has become one of the most well studied regions in the Transhimalaya with research focusing on glaciation (Fort, 1983; Burbank and Fort, 1985; Brown et al., 2002; Damm, 2006; Owen et al., 2006; Dortch et al., 2010a), the development of asymmetrical topography (Jamieson et al., 2004; Kirstein, 2011; Dortch et al., 2011a) and valley morphology (Hobley et al., 2010; Reynhout et al., 2013), the importance of large landslides in landscape development (Dortch et al., 2009), exhumation histories (Dunlap et al., 1998; Kirstein et al., 2006, 2009; Kumar et al., 2007), strath terraces development, and catastrophic flooding (Brown et al., 2003; Dortch et al., 2011a,b; Hobley et al., 2012). A common theme in many of these studies is the underlying importance of glaciation in influencing landscape development (Hobley et al., 2010; Dortch et al., 2011a; Reynhout et al., 2013).

To produce a coherent glacial chronostratigraphic framework for an extensive region of the Himalayan–Tibetan orogen we present a new glacial chronostratigraphy for Ladakh using cosmogenic  $^{10}\text{Be}$  dating. We compare this chronology with published chronologies for semi-arid regions to the north and south. This framework provides a foundation for future Quaternary paleoenvironment, landscape development and tectonic studies.

## 2. Study area

The study region spans the semi-arid mountain regions at the western end of the Himalayan–Tibetan orogen and includes the Transhimalaya, greater Himalaya, Pamir, and Tian Shan (Fig. 1). Within this region there are several relatively isolated massifs, which include Mustag Ata, Kongur Shan, and Nun-Kun. The mountains are among the highest in the world and include five 8000 m-high peaks (K2 at 8611 m above sea level [asl], Nanga Parbat at 8126 m asl, Gasherbrum 1 at 8068 m asl, Broad Peak at 8047 m asl, and Gasherbrum II at 8035 m asl). The high topography was produced by the collision of the Indian–Asian continental lithospheric plates starting at  $\sim 50$  Ma, which resulted in  $\sim 2000$  km of crustal shortening (Dewey et al., 1989; Johnson, 2002). This is one of the most glaciated regions outside of the polar realm and includes glaciers that exceed many tens of kilometers in length. The climate of the region is influenced by both the mid-latitude westerlies and Indian monsoon (Benn and Owen, 1998). Lehmkühl and Owen (2005), Owen et al. (2005, 2012) and provide overviews of the Quaternary glaciation of the Himalayan–Tibetan orogen.

The detailed study area focuses on the Ladakh and Pangong ranges that trend NE–SW within the Transhimalaya. The Ladakh and Pangong ranges rise from about 3500 m asl to peaks reaching  $>6000$  m asl, and contain deeply incised valleys with 1–3 km of relief. The Ladakh Range is bounded to the south by the Indus–Tsangpo suture zone and to the north by the Shyok suture zone and Karakoram Fault. The range experienced rapid exhumation during the Oligocene, and slow exhumation on the northern side of the range since the Miocene (Kirstein et al., 2006, 2009, 2011; Dortch et al., 2011a). The Pangong Range is bounded by two strands of the Karakoram fault and has undergone exhumation during two periods of transpression at 13–17 Ma and 7–8 Ma (Dunlap et al., 1998).

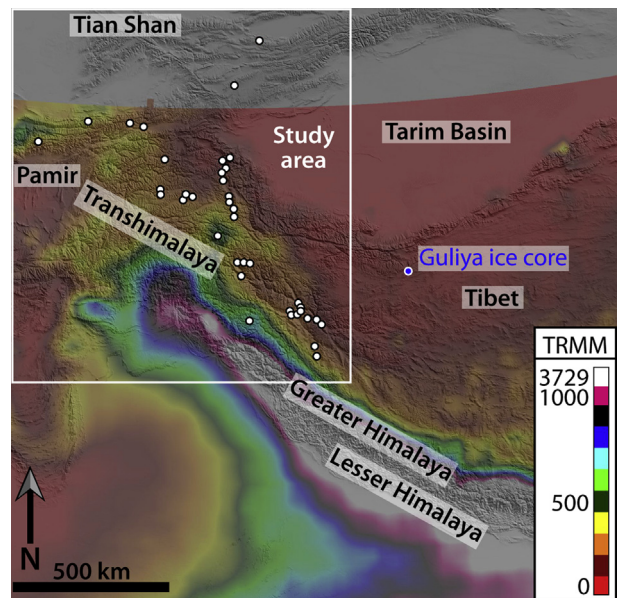


**Fig. 1.** Shuttle radar topography mission (SRTM) hillshade digital elevation model (DEM) of the western portion of the Himalayan–Tibetan orogen. Tropical Rainfall Measurement Mission (TRMM) average annual precipitation data for 1998–2008 (from Bookhagen and Burbank, 2006; Bookhagen, 2013) is superimposed on the DEM. Sample locations for all studies are denoted by white dots while the location of Guliya ice core is denoted by a blue dot. Location of Fig. 12 is outlined by a white box. (For interpretation of the references to color in this figure legend, the reader is referred to the web version of this article.)

The Ladakh and Pangong ranges, and the Zaskar Range to the south, receive most of their precipitation from the Indian summer monsoon (Gasse et al., 1996; Brown et al., 2003; Owen et al., 2006). In contrast, the Karakoram Range and the Pamir to the north receives the majority of its precipitation from the mid-latitude westerlies (Miehe et al., 2001). The strength of the monsoon and mid-latitude westerlies, along with precipitation gradients, have changed over time due to changes in insolation influenced by variations in the Earth orbital parameters (Gasse et al., 1996; Benn and Owen, 1998; Bookhagen et al., 2005; Demske et al., 2009). Currently, the region is characterized as semi-arid, and receives  $\leq 200$  mm of precipitation per year (Bookhagen and Burbank, 2006; Bookhagen, 2013).

Brown et al. (2002) and Owen et al. (2006) defined the timing of glaciation for the southern side of the Ladakh Range using cosmogenic  $^{10}\text{Be}$  dating, and Dortch et al. (2010a, 2011a,b) made tentative correlations of glacial landforms across the Ladakh Range and the Nubra, Shyok, and Tangtse river valleys. To the north and south of the study area, Owen et al. (2002, 2012), Zech et al. (2005a, 2013), Abramowski et al. (2006), Seong et al. (2007, 2009c), Koppes et al. (2008), Hedrick et al. (2011), Zech (2012), Röhringer et al. (2012) and Lee et al. (2013) defined the timing of glaciation using  $^{10}\text{Be}$  methods.

## 3. Methods

### 3.1. Field methods

All landforms were mapped in the field aided by remote sensed imagery, which included panchromatic merged 15 m Landsat ETM+ and 3 arc-second [90 m] Shuttle Radar Topography Mission [SRTM] DEMs (CGIAR-CSI, 2007; USGS EarthExplorer, 2011; Fig. 2). Five valleys in the Ladakh Range and one valley in the Pangong Range were traversed and mapped in detail.

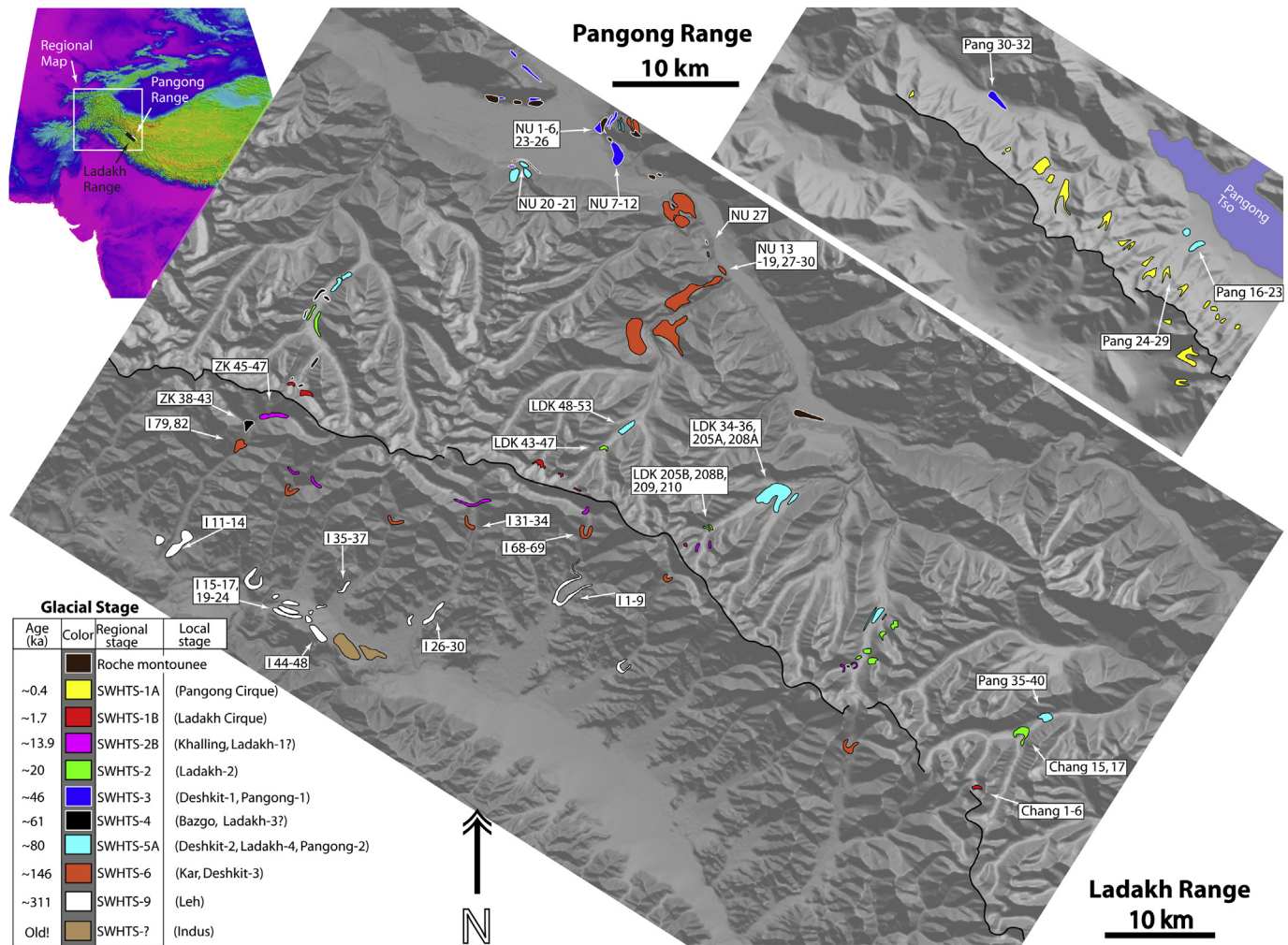


**Fig. 2.** Geomorphic maps of the Ladakh and Pangong ranges on hillshaded SRTM DEMs. Inset in top left shows location of Ladakh and Pangong ranges. Thin Black line denotes the Ladakh and Pangong range divides. Glacial stages from previous studies (Owen et al., 2006; Dortch et al., 2010a) for the southern sides of the Ladakh and Karakoram ranges are included. Names and locations of boulder samples for this and previous studies are marked for each landform sampled for  $^{10}\text{Be}$  dating. Various colors are assigned to each correlative glacial stage and approximate glacial stage ages are listed in stratigraphic order in the key. (For interpretation of the references to color in this figure legend, the reader is referred to the web version of this article.)

### 3.2. Morphostratigraphy

We used the methods discussed in detail in Owen et al. (1998, 2011, 2012), Hughes et al. (2005), and Seong et al. (2009c) to develop a morphostratigraphy and hence a glacial chronostratigraphy for our study area. Glacial and associated landforms were mapped based on their morphostratigraphic positions and relationships, and the relative weathering of their forms and surfaces. Glacial stages were assigned to distinct sets of landforms with similar morphostratigraphic positions and relative weathering characteristics. Using glacial stage names to correlate glacial landforms throughout a region does not imply a numerical age for the particular glacial stage. As in Owen et al. (1998, 2011, 2012) and Seong et al. (2009c), this approach is used to provide a framework for sampling for  $^{10}\text{Be}$  dating to help define the numerical ages for the glacial stages. Once numerical ages were determined on landforms a chronostratigraphy was established.

### 3.3. $^{10}\text{Be}$ dating

Approximately 500 g of rock were collected from each of the selected boulders on landforms for  $^{10}\text{Be}$  dating. Topographic

shielding was measured using a handheld inclinometer at 15 intervals for the azimuths. Quartz isolation, dissolution, chromatography, isolation of Be, and preparation of BeO were undertaken in the geochronology laboratories at the University of Cincinnati following the methods of Kohl and Nishiizumi (1992), and described in detail in Dortch et al. (2009). Ratios of  $^{10}\text{Be}/^9\text{Be}$  were measured using accelerator mass spectrometry at the Purdue Rare Isotope Measurement Laboratory at Purdue University (Appendix A).

All ages were calculated using the CRONUS-Earth online calculator Version 2.2 applying appropriate  $^{10}\text{Be}$  standardizations (Appendix A). We report internal and external uncertainty and the time independent result using Lal (1991) and Stone (2000) scaling scheme following the documentation of Balco et al. (2008). Six hundred and forty-eight previously published  $^{10}\text{Be}$  ages were recalculated using the same scheme to allow direct comparisons to be made with the new data (Appendix A).

No standard for geomagnetic correction has been agreed upon within the  $^{10}\text{Be}$  dating community (cf. Balco et al., 2008; Owen et al., 2008). Variance between ages calculated by different scaling for geomagnetic correction is greatest for the oldest landforms (Lifton et al., 2005). For example, a 350 ka landform will be affected by as much as ~100 ka using the time-independent model

of Lal (1991) and Stone (2000) versus Lifton et al. (2005) schemes. In contrast, the discrepancy is small for younger ages; for example, for ages of  $\sim 17$  ka the difference is  $\sim 4\%$ . Variations due to the scaling model for young ages (stages) will not change our climatostratigraphic correlations. These issues are specifically addressed for the Himalayan–Tibetan orogen by Owen et al. (2008) and Owen and Dortch (2013).

Recent studies focused on refining  $^{10}\text{Be}$  production rates have a regional Holocene focus and are based on landforms of “known” age determined through  $^{14}\text{C}$  methods. We refer the reader to Briner et al. (2012), Goehring et al. (2012), and references therein for more detail. This approach has not specifically been carried out with regards to the Himalaya–Tibetan orogen; an extrapolation to our study area is more uncertain than the global referenced model used by Version 2.2 of the CRONUS–Earth online calculator. Thus, systematic changes in production rate cannot be adequately accounted for the Himalayan–Tibetan orogen at this time. More importantly, scattering of ages due to geologic uncertainty far outweighs geomagnetic and production rate uncertainty. For example, of the 70 separated gaussians used in this study: 49 have errors at  $2\sigma$  that encompass 10–15% production rate error; 6 with smaller errors are occur after the global Last Glacial Maximum (gLGM) thus 10–15% production rate error would not affect climatic correlations; the remaining 15 are only tentatively linked with climatic records as they are pre-gLGM.

## 4. Age statistics

### 4.1. Local glacial stages

Age results from individual samples are combined for each local glacial stage. Results are combined with previous studies following the interpretations of the earlier studies.

Analysis of  $^{10}\text{Be}$  ages usually involves quantitatively describing the clustering of ages on a particular surface. Statistical methods vary by study and commonly include reduced chi-squared or mean square weighted deviates, probability density functions (PDFs), and  $2\sigma$  test (Douglass et al., 2006; Ivy-Ochs et al., 2007; Chevalier et al., 2011; Heyman et al., 2011). In this study, we separate gaussians from the cumulative PDFs using the “ksdensity” kernel in MATLAB 2011a in a model (Fig. 3). The model uses a dynamic smoothing window based on internal errors to prevent over- or under-smoothing of the  $^{10}\text{Be}$  age data during generation of the cumulative PDF. Internal errors are used to prevent production rate uncertainties interfering with the clustering of ages at nearby sites (Applegate et al., 2010). Thus, our model takes both the error and the distribution of the individual  $^{10}\text{Be}$  measurements into account during generation of the cumulative PDF. PDF peaks and tails are then separated into individual gaussians, the sum of which integrates to the cumulative PDF at 1000 iterations to obtain the best fit. The re-integrated PDF (made from the isolated gaussians) goodness of fit is indicated graphically (individual figures for all local glacial stages used are available in Appendix B and C while figures for omitted local glacial stages are available in Appendix D). Some separated gaussians are wider than would be expected if only measurement uncertainties and moraine stabilization affects the remaining age distributions. However, there is no way to determine if the remaining scatter is due to inheritance or exhumation processes since outliers have already been removed. Thus, we report the age by using the gaussian peak and the uncertainty (clustering of  $^{10}\text{Be}$  ages) by gaussian standard deviation ( $1\sigma$ ) values.

In this study, we set the criteria that a gaussian must enclose a minimum of three ages to define a glacial stage. We use three ages as the limit because geologic uncertainty scatters ages and if

boulders are approximated as roughly tabular, there is a 50% probability for one age, 25% probability for two ages, and 12.5% probability for three ages to give an incorrect average. Using three ages as a minimum to set the age of a glacial stage is more statistically strict than many studies undergoing reanalysis. The probability that three ages are similar and fit the expected normal distribution and still yield an incorrect age is  $\ll 12.5\%$ . Gaussians enclosing 2 exposure ages are considered tentative, and gaussians containing a single age unreliable. Hence, we limit the  $^{10}\text{Be}$  dataset to the most reliable results.

Denudation and inheritance have been shown to have significant affect on the clustering of ages on old and young moraines, respectively (e.g. Putkonen and Swanson, 2003; Putkonen and O’Neal, 2006; Seong et al., 2009d). Thus, we adapt two interpretation schemes for old and young moraines to address these issues as discussed in the next two subsections. We use the gLGM, as defined by Mix et al. (2001), as the delineation between old and young moraines as the global glacial event is generally well identified and well preserved compared to older glacial debris.

#### 4.1.1. (post) gLGM moraines

Moraines and individual boulder surfaces degrade over time (Putkonen and Swanson, 2003; Zech et al., 2005b; Putkonen and O’Neal, 2006), and inheritance of  $^{10}\text{Be}$  in Himalayan glacial debris has been shown to be less significant than effects due to moraine degradation and surface weathering (Heyman et al., 2011). To simultaneously account for geologic scatter while still excluding outliers on landforms older than 21 ka, we interpret the oldest gaussian that contains  $\geq 3$   $^{10}\text{Be}$  ages as the most likely approximation for a local glacial stage and older gaussians with  $< 3$   $^{10}\text{Be}$  ages as inherited outliers. See Fig. 3 for an example plot and flow chart describing our method in detail.

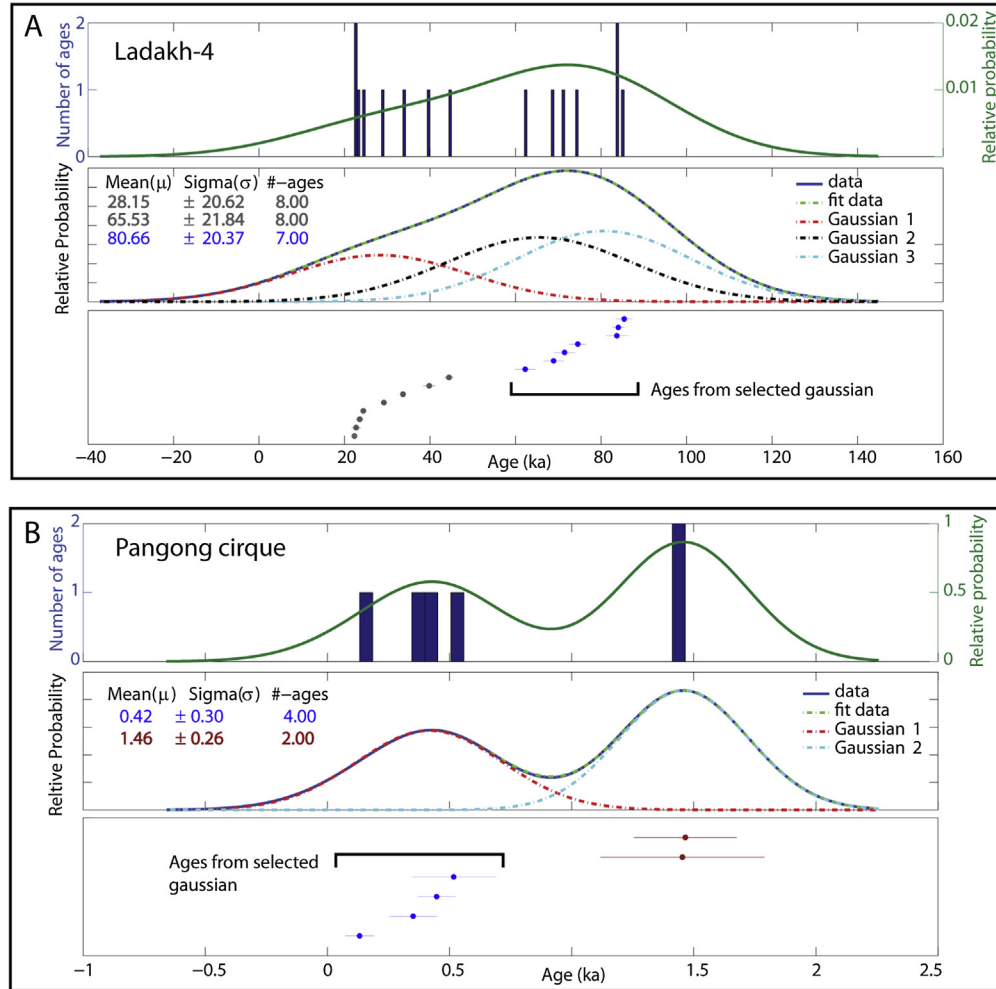
#### 4.1.2. gLGM and younger moraines

gLGM and younger moraines are typically well preserved with less moraine or boulder surface degradation than older moraines. Younger moraine ages can be significantly influenced by small amounts of inheritance (1–5 ka). Moraines may take 1300–2000 years to stabilize, during which time erosion may play a significant role (Putkonen and Swanson, 2003; Briner et al., 2005; Putkonen and O’Neal, 2006; Ivy-Ochs et al., 2008; Dortch et al., 2010b), leading to younger ages. We follow Applegate et al. (2010) and take the highest probability gaussian as the best approximation of the local glacial stage age (Fig. 3). This approach excludes samples with notable inheritance as well as boulders that have experienced some degree of erosion or instability.

### 4.2. Regional glacial stages

Initially, the ages of local glacial stages were examined and grouped graphically. The  $^{10}\text{Be}$  ages enclosed by the chosen gaussians were then compared using Student’s *t*-test to determine if the different local glacial stages are distinct (*p*-value of  $\leq 0.05$ ), or if they potentially belong to a normal distribution (*p*-value of  $> 0.05$ ) that would be expected from regional glaciation. The  $^{10}\text{Be}$  ages from local glacial stages that could be part of a single normal distribution were combined to form a regional glacial stage dataset. The regional stage datasets were then compared using Student’s *t*-test a second time. All of the regional glacial stage clusters presented here have *p*-values of  $\leq 0.01$  (i.e. are distinct groupings at  $\geq 99\%$  confidence level) except for SWHTS 2C (*p*-value of 0.04), which is distinguished at  $> 95\%$  confidence level. Regional glacial stage ages are defined using the mean and mean absolute deviation (MAD) of the combined pool of individual  $^{10}\text{Be}$  ages. A simple mean of the separated gaussians cannot be used since the degree

## Gaussian separation example figures



## Gaussian separation flow chart

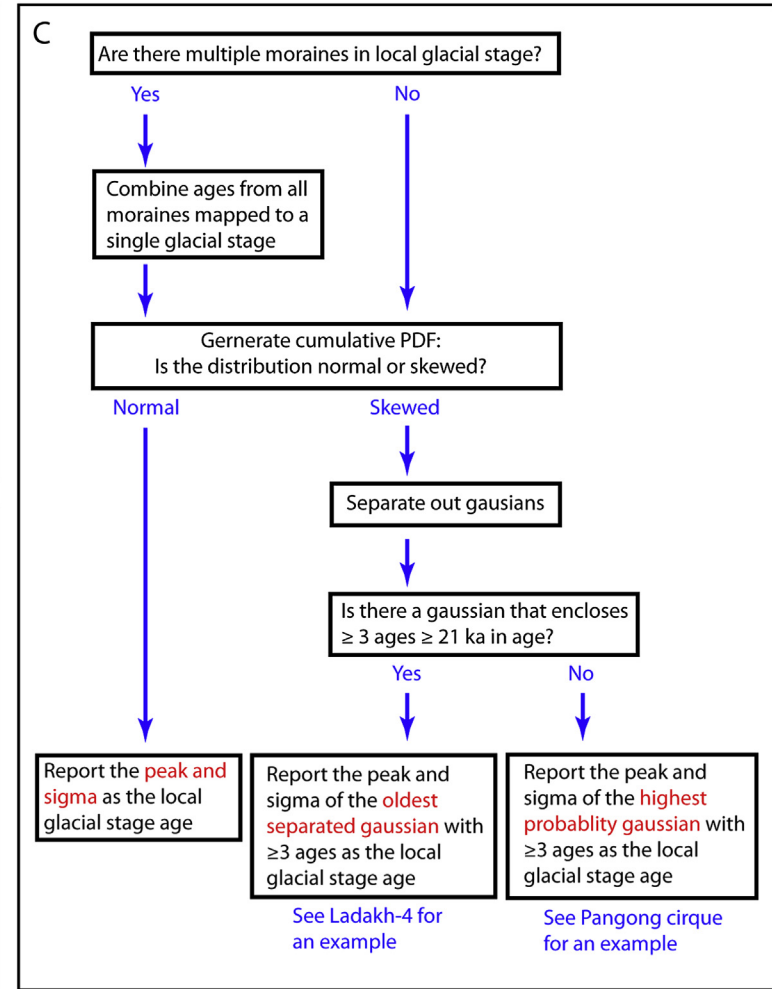


**Fig. 3.** Example of our gaussian separation method on two moraines, (A) pre-gLGM (Ladakh-4) and (B) post-gLGM (Pangong cirque). Ages and  $1\sigma$  values for gaussians are listed in the middle of both examples. Enclosed  $^{10}\text{Be}$  ages and corresponding peak age and error are highlighted by blue dots and text, respectively. Gray dots represent  $^{10}\text{Be}$  ages that are too young (exhumed), and red dots too old (inherited). (C) Flow chart provides details of our method of separating and interpreting gaussians. (For interpretation of the references to color in this figure legend, the reader is referred to the web version of this article.)

of scattering between each gaussian is different. Standard deviation requires each gaussian to have similar deviations and the combined  $^{10}\text{Be}$  age dataset to be distributed normally. These conditions will rarely be satisfied. Thus, MAD is the preferred estimator of error in this study as absolute deviations from the mean provide increases robustness in dealing with outliers and non-normal distributions.

## 5. Landform description

### 5.1. Ladakh Range

Five valleys were studied in detail on the northern side of the Ladakh Range. Five sets of moraines were distinguished, which we assign to the Ladakh Cirque (youngest), Ladakh-1, Ladakh-2, Ladakh-3 and Ladakh-4 (oldest) glacial stages (Fig. 2).

Terminal and lateral moraines from the Ladakh-4 stage are present in all five mapped valleys (Figs. 2 and 4). They are  $8.5 \pm 1.3$  km from the range divide and are located in the north facing trunk valleys. Unlike the sharp crested moraines south of the divide (c.f. Owen et al., 2006), Ladakh-4 glacial stage moraines are hummocky, and despite numerous small-incised channels, generally fill valley bottoms.

There are numerous large boulders (>1 m tall) with light gray to buff patchy varnish on the moraine (Fig. 4). These boulders comprise medium to coarse grained diorite, and are undergoing granular disintegration and salt crystal weathering. Most of the large boulders have “knobs” protruding 2–5 cm above the surface that are both exceptionally hard and unweathered compared to the rest of the boulder surface, or are capped by substantially more mafic fine grained rock that is more resistant to

weathering. A total of 16 samples from 3 moraines in 3 valleys were collected from knobs and flat boulder surfaces for  $^{10}\text{Be}$  dating (labeled in Fig. 2).

Ladakh-3 glacial stage moraine is only present in one valley on the western end of the Ladakh Range (Fig. 2). The main body of the latero-frontal moraine is located on the west side of the valley, with remnants preserved on the east side. This is a composite moraine with at least two distinguishable crests. Boulders have similar weathering characteristics and have the same protruding knobs as the Ladakh-4 stage boulders. Samples from this moraine were not processed.

Hummocky latero-frontal moraines for the Ladakh-2 stage are present in all five valleys (Figs. 2 and 5). They are smaller, less eroded, and have few incised channels compared to Ladakh-4 stage moraines. Ladakh-2 stage moraines are located  $5.2 \pm 1.0$  km from the range divide and are typically restricted to the confluence of tributary valleys.

Despite the better preservation of the moraines, large boulders (>1 m-tall) have similar weathering characteristics and have the same protruding knobs as the Ladakh-4 stage boulders (Fig. 5). A total of 11 samples from 3 moraines in 3 valleys were collected from knobs and flat boulder surfaces for  $^{10}\text{Be}$  dating.

The Ladakh-1 stage moraines are located in the uppermost tributaries in two of the five valleys traversed  $\sim 2.5 \pm 0.4$  km from the range divide (Fig. 2). These small terminal moraines have a hummocky surface with fresh angular boulders and lack visible signs of moraine or boulder weathering. Samples from these moraines were not processed for dating.

Moraines of the Ladakh Cirque glacial stage are present in three valleys juxtaposed to modern cirque glaciers (Figs. 2 and 6). The moraines have a moderately hummocky surface and comprise

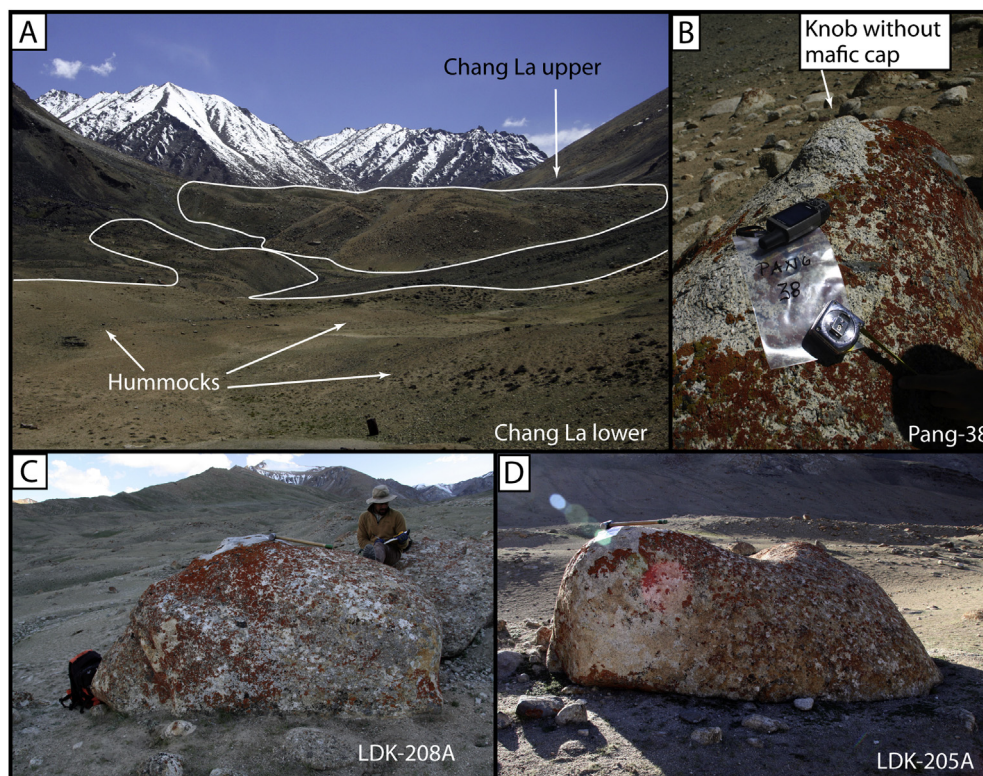


**Fig. 4.** View of Ladakh-4 glacial stage moraine (A) and selected boulders (B, C, and D). (A) View looking south of Chang La lower moraine hummocks (foreground) and Chang La upper (Ladakh-2; background) are outlined in white. (B) Knob on top of the Chang La lower moraine boulder and GPS for scale. Boulders in (C) and (D) are from the Diger La lower moraine.

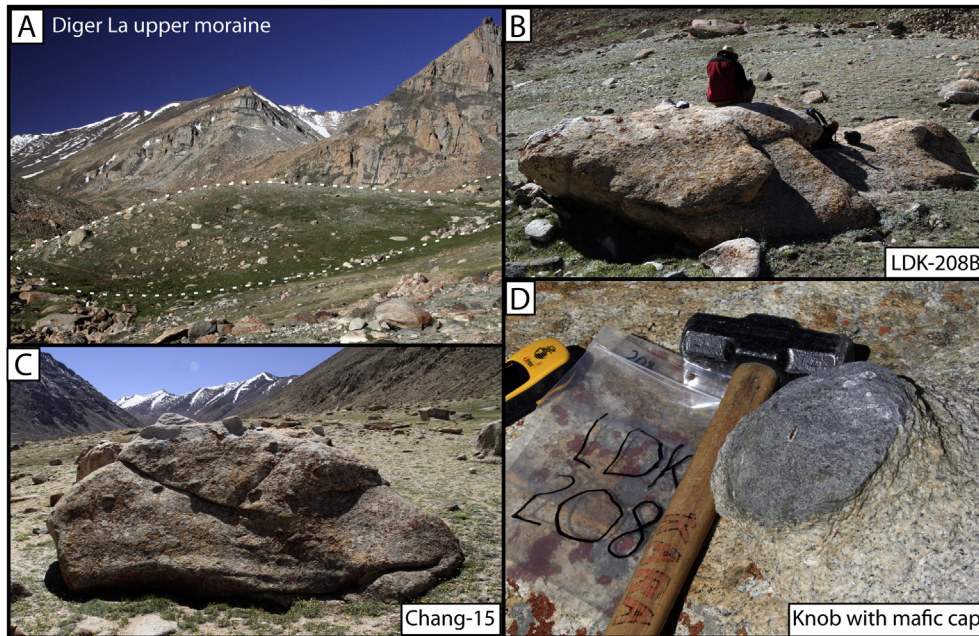


**Fig. 5.** North view of the Diger La upper moraine of the Ladakh-2 glacial stage (A) and selected boulders (B, C, and D). Boulder in (B) is from the Diger La upper moraine while the boulder in (C) is from the Chang La upper moraine. (D) Knob with a fine grained mafic cap on top of boulder pictured in (B) with Kara the hammer for scale.

fresh, hard, angular blocks. There is no evidence of weathering and no protruding knobs are present. Six samples were collected from a single moraine for  $^{10}\text{Be}$  dating.

### 5.2. Pangong Range

Valleys in the Pangong Range are significantly shorter and steeper than those in the Ladakh Range. Slope processes dominate sediment flux and rework glacial deposits in trunk valleys. Two sets of moraines were identified in addition to roche moutonnées mapped by Dortch et al. (2011b) that we assign to the Pangong Cirque (youngest), Pangong-1, and Pangong-2 (oldest) glacial stages.

The Pangong-2 glacial stage is represented by a set of paired moraines that have distinct ridge crests that merge up valley (Figs. 2 and 7). The crest is rounded and deflation of the moraine is indicated by boundaries in the degree of varnish on the sides of boulders (Fig. 7B). There is no discernible difference between the

morphology of the inner and outer moraines. Boulders on the moraines are  $<1$  m in any dimension, have rock varnish that ranges from patchy dark brown to patchy buff. The boulders comprise gneiss and granite with granular disintegration and fracturing controlled weathering. Eight samples were collected from boulders on the paired moraines for  $^{10}\text{Be}$  dating.

Evidence for the Pangong-1 glacial stage is confined to sparse preserved patches of till present between the paired Pangong-2 moraines and the recent Pangong Cirque moraines (Fig. 8B). These sediments are distinct from slope sediments and are interpreted as a degraded glacial landform, which may represent at least one intermediate glacial advance or recessional stand still following the deglaciation of the Pangong-2 glacial stage. Unfortunately these sediments were not suitable for  $^{10}\text{Be}$  dating.

Up valley, there is a substantial ice-contact moraine (Pangong Cirque glacial stage) composed of fresh, hard, angular gneiss and granite blocks (Fig. 8). The moraine has a moderately hummocky surface and there is no evidence of secondary weathering. Six samples were collected for  $^{10}\text{Be}$  dating from the crests of hummocks.

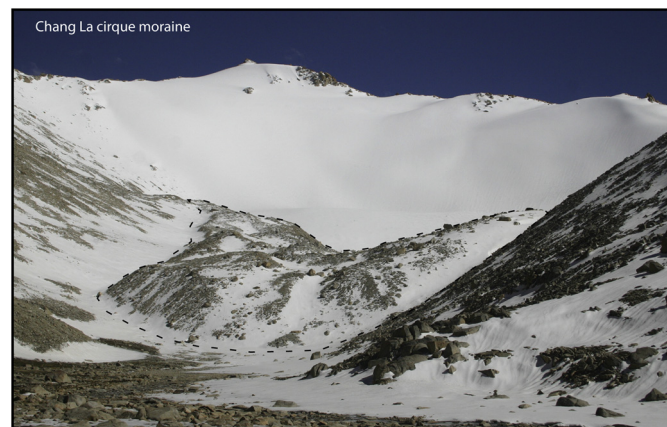


**Fig. 6.** East view of Chang La cirque moraine (Ladakh Cirque glacial stage) freshly covered by summer snows.

## 6. Results for Ladakh and Pangong ranges

Ages for the glacial stages from the Ladakh and Pangong ranges are discussed below in chronological order. Individual ages and figures for all glacial stages used are presented in Table 1, and Appendices B and C.

### 6.1. Moraines older than 21 ka

Field observations show that moraines of the Pangong-2 glacial stage are eroded; the cumulative PDF peak is skewed toward the younger ages. The oldest gaussian isolated out of the old PDF tail has a peak age of  $85 \pm 15$  ka (uncertainty =  $1\sigma$ ) and encloses three ages. We interpret  $85 \pm 15$  ka to represent the best estimate of the age for this glacial stage.

Three gaussians were separated out of the combined Ladakh-4 glacial stage moraine  $^{10}\text{Be}$  ages. The two gaussians isolated out of

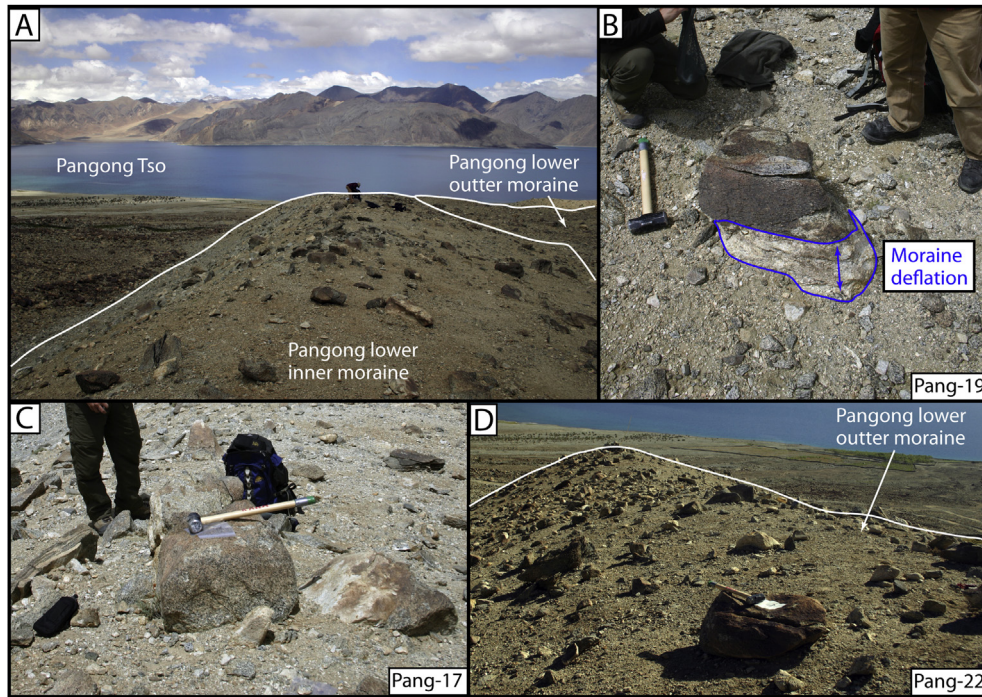


**Fig. 7.** North view of Pangong lower inner and lower outer paired moraines (A and D) and boulders (B, C, and D) of the Pangong-2 glacial stage. Note the sharp change in rock varnish outlined in blue (B). Kara the hammer's handle is 50 cm long. (For interpretation of the references to color in this figure legend, the reader is referred to the web version of this article.)

the young tail of the skewed PDF indicate that moraines and/or boulders from this stage have been weathered, which agrees with our field observations. The oldest gaussian peak is  $81 \pm 20$  ka for seven  $^{10}\text{Be}$  ages and is interpreted to represent the best age estimate of the age for the Ladakh-4 glacial stage.

The cumulative PDF of Ladakh-2  $^{10}\text{Be}$  ages is trimodal due to poorly clustered old ages. The oldest two ages separate the gaussians contain less than three ages each; thus the enclosed  $^{10}\text{Be}$  ages

are interpret as inherited outliers. The gaussian at  $22 \pm 3$  ka encloses seven  $^{10}\text{Be}$  ages and is interpreted to best represent the age of the Ladakh-2 glacial stage.

### 6.2. Moraines younger than 21 ka

There are three separate gaussians in the cumulative PDF for the  $^{10}\text{Be}$  ages for the Ladakh Cirque glacial stage. The oldest two

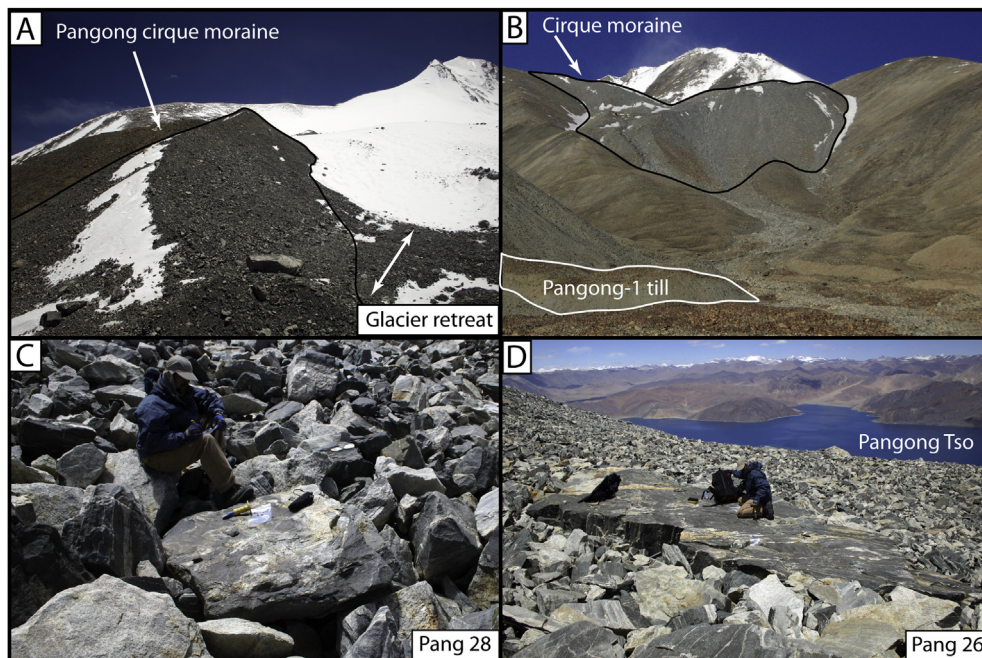


**Fig. 8.** South view of Pangong cirque moraine (A and B) of the Pangong cirque glacial stage. (B) The cirque moraine is outlined in black while patches of Pangong-1 glacial stage till is visible in the foreground and outlined white. (C and D) South view of boulders selected for  $^{10}\text{Be}$  dating.

**Table 1**  
 Details of local and regional glacial stages including name, age, *p*-values, and suggested climate correlations. Column four represents the range of *p*-values when testing clusters of <sup>10</sup>Be ages between local glacial stages. All *p*-values are greater than 0.05 which suggest there is no reason to reject the null hypothesis and that the local glacial stages may belong to a single normal distribution. Column six contains *p*-values for the comparison of combined regional glacial stage <sup>10</sup>Be age sets. Here, *p*-values less than 0.05 indicates that the regional <sup>10</sup>Be age sets are distinct and separate at ≥95% confidence level. Note, the *p*-values comparing PM-2 are >0.05 due to significant scatter of the <sup>10</sup>Be ages (see text for details).

Regional glacial stage	Local Glacial stage	Local stage age (ka)	P-values between local glacial stages	Regional stage age (ka)	P-values between regional glacial stages	Climate correlation
SWHTS 9	Karasu stage of Seong et al., 2009c	371±65	0.86-0.94	311±32	0.00	N/A MIS 9/10
	Leh stage of Owen et al., 2006	317±57				
	KM-0 stage of Hedrick et al., 2011	311±8				
SWHTS 7 [tentative]	Dabudaer stage of Owen et al., 2012	234±44	N/A	234±44	0.01	MIS-7/8 [tentative]
SWHTS 6	Deshket 3 stage of Dortch et al., 2009	156±16	0.42-0.92	146±18	0.01	MIS-6, Monsoon & Westerly
	Skardu stage of Seong et al., 2007	153±30				
	Kar stage of Owen et al., 2006	151±46				
SWHTS 5E	Subaxh stage of Seong et al., 2009	128±19	0.55-0.71	121±11	0.00	MIS-5e, Monsoon
	PM-0 stage of Hedrick et al., 2010	126±8				
	Terskey ala Tau II stage of Koppes et al., 2008	123±31				
SWHTS 5A	Deshket 2 stage of Dortch et al., 2009	86±4	0.28-0.69	80±5	0.00	MIS-5a; Monsoon
	Pangong-2 stage (this study)	85±15				
	M1 stage of Zech et al., 2005	83±2				
	Ladakh-4 stage (this study)	81±20				
	TK stage of Abramowski et al., 2006	80±3				
SWHTS 5A-	UK3 stage of Abramowski et al., 2006	73±16	0.69-0.88	72±8	0.00	MIS 4/5a; Monsoon/recession
	Tashkurgan stage of Owen et al., 2012	73±10				
	KM 1-3 stage of Hedrick et al., 2011	72±31				
	BO1 stage of Abramowski et al., 2006; Röhringer et al., 2012	70±8				
SWHTS 4	KK stage of Abramowski et al., 2006	66±7	0.40-0.99	61±5	0.00	MIS-4; Westerly; Heinrich event-6
	M2 stage of Zech et al., 2005	64±22				
	Terskey ala Tau III stage of Koppes et al., 2008	62±4				
	G8 stage of Zech et al., 2013	62±2				
	Borit Jheel stage of Owen et al., 2002	60±4				
	Bazgo stage of Owen et al., 2006	60±14				
	Kitsch-Kurumdu 6 stage of Zech et al., 2012	59±5				
Achambur stage of Lee et al., 2013	57±7					
SWHTS 3	Deshkit 1 stage of Dortch et al., 2009	48±4	0.42-0.68	46±4	0.00	MIS-3; Monsoon; Heinrich event-5
	PM-1 stage of Hedrick et al., 2011	47±12				
	Pangong-1 stage of Dortch et al., 2011	40±3				
SWHTS 2F	Hangdi stage of Owen et al., 2012	33±4	0.10-0.94	30±3	0.00	MIS-2; Monsoon; Heinrich event-3
	Guhulki 1 stage of Owen et al., 2002	28±3				
	GU2 stage of Abramowski et al., 2006	28±8				
	M4 stage of Zech et al., 2005	28±0.3				
SWHTS 2E	Ladakh-2 stage (this study)	22±3	0.32-0.97	20±2	0.00	MIS-2; Westerly; gLGM
	BO2 stage of Abramowski et al., 2006	22±0.3				
	AK4 stage of Abramowski et al., 2006	22±1				
	G5 stage of Zech et al., 2013	21±0.8				
	AT stage of Abramowski et al., 2006	20±4				
	G1 stage of Zech et al., 2013	20±0.3				
	Tarangoz Tongul stage of Lee et al., 2013	19±2				
	Kuzigun stage of Owen et al., 2012	19±6				
	UK5 stage of Abramowski et al., 2006	18±1				
	Olimde 1 stage of Seong et al., 2009	18±1				
SWHTS 2D	Kitsch-Kurumdu 3 stage of Zech et al., 2012	17±2.6	0.44	16.9±0.7	0.00	MIS-2; Westerly; Oldest Dryas; Heinrich event-1
	Mungo 1 stage of Seong et al., 2007	16.6±0.3				
SWHTS 2C	Anantick-Tongul stage of Lee et al., 2013	15.6±1.4	0.86	14.9±0.8	0.04	MIS-2; Westerly; Late Oldest Dryas
	Kitsch-Kurumdu 2 stage of Zech et al., 2012	15.6±1.1				
SWHTS 2B	Khalling stage of Owen et al., 2006	14.7±3.0	0.68	13.9±0.5	0.00	MIS-2; Westerly; Older Dryas
	Olimde 2 stage of Seong et al., 2009	14.0±0.7				
SWHTS 2A	AV stage of Abramowski et al., 2006	12.3±0.2	0.55-0.91	12.2±0.8	0.00	MIS-2; Westerly; Younger Dryas
	Mungo 2 stage of Seong et al., 2007	12.2±1.0				
	Batura stage of Owen et al., 2002	11.8±1.9				
	Anantick stage of Lee et al., 2013	11.8±3.2				
	BO8 stage of Röhringer et al., 2012	11.6±1.2				
SWHTS 1E	Olimde 3 stage of Seong et al., 2009	8.8±0.3	N/A	N/A	0.00	MIS-1; Monsoon peak1; Climatic Optimum [tentative]
SWHTS 1D	Olimde 4 Stage of seong et al., 2009	6.9±0.2	N/A	N/A	0.00	MIS-1; Climatic Optimum [tentative]
Correlation inconclusive	Askole 1 stage of Seong et al., 2007	5.5±0.7	N/A	N/A	0.00	MIS-1; Climatic Optimum [tentative]
SWHTS 1C	Olimde 5 stage of Seong et al., 2009	4.0±0.1	0.39-0.73	3.8±0.6	0.28	MIS-1; Westerly
	Askole 2 stage of Seong et al., 2007	4.0±0.5				
	KM-4 stage of Hedrick et al., 2011	3.9±1.6				
	Olimde 6 stage of Seong et al., 2009	3.4±0.4				
Correlation inconclusive	PM-2 stage of Hedrick et al., 2011	2.7±2.3	N/A	N/A	0.21	MIS-1; Monsoon; Roman Humid period
SWHTS 1B	Ladakh Cirque (this study)	1.8±0.4	0.20	1.7±0.2	0.00	MIS-1; Monsoon; Roman Humid period
	Olimde 7 stage of Seong et al., 2009	1.6±0.4				
Correlation inconclusive	Askole 3 stage of Seong et al., 2007	1.0±0.3	N/A	N/A	0.00	MIS-1; Westerly; Little Ice Age
SWHTS 1A	Lomp stage of Lee et al., 2013	0.5±0.1	0.48-0.52	0.4±0.1	N/A	MIS-1; Westerly; Little Ice Age
	Olimde 8 stage of Seong et al., 2009	0.5±0.2				
	Pangong Cirque (this study)	0.4±0.3				
	PM-3 stage of Hedrick et al., 2011	0.3±0.2				

separated gaussians enclose a single inherited age each and have probabilities of  $\leq 0.35$ . The youngest gaussian has the highest probability (0.6) at  $1.8 \pm 0.4$  ka, contains four ages, and is considered to be the best representation of the most recent glaciation on the northern side of the Ladakh Range.

The cumulative PDF for the  $^{10}\text{Be}$  ages for the Pangong Cirque glacial stage is bimodal. The oldest gaussian has the highest probability (0.8). However, it only encloses two ages and hence we interpret them as inherited  $^{10}\text{Be}$  ages. The younger gaussian at  $0.4 \pm 0.3$  ka encloses four  $^{10}\text{Be}$  ages and is interpreted as the most likely age for this glacial stage.

## 7. Regional analysis of glacial ages

A regional synthesis was undertaken by recalculating 645  $^{10}\text{Be}$  ages from Owen et al. (2002, 2012), Zech et al. (2005a, 2013), Abramowski et al. (2006), Seong et al. (2007, 2009c), Koppes et al. (2008), Hedrick et al. (2011), Dortch et al. (2010a, 2011b), Zech (2012), Röhringer et al. (2012) and Lee et al. (2013). Individual graphs for all 70 glacial stages used are available in Appendix B and C. When two or more local glacial stages have statistically indistinguishable ages ( $p$ -values of  $>0.05$ ), we use the mean and MAD of the  $^{10}\text{Be}$  ages enclosed by selected gaussians to define a regional glacial stage. A local glacial stage dated in more than one valley within a single range is highlighted as tentative with speculative correlation to climatic records; a local glacial stage in a single valley is highlighted as having an inconclusive climatic correlation.

Analysis of the  $^{10}\text{Be}$  ages results in 16 clusters of ages that include 64 local glacial stages. An additional three tentative regional glacial stages are highlighted along with three local glacial stages whose relationship to regional or climatic events remains inconclusive due to either large error or paucity of landforms at a similar age. We recognize that our local glacial stage and regional stage averages for moraines  $>21$  ka in age are minimum estimates, and use this information when drawing tentative climatic linkages. In contrast, local glacial stage and regional stage averages for moraines  $<21$  ka in age are directly comparable to climatic records.

No age was determined for the UK1, UK6, G7, BO5, BO6, BO7, Terskey Ala Tau IV, Terskey Ala Tau V, Ferghana range III, Aksai-AtBashi III, AtBashi II, Kitschi-Kurumdu 7, and Aksai IV-V moraines due to insufficient number of  $^{10}\text{Be}$  ages preventing analysis. Ages for AK1, AK2, AK3, GU1, Indus, UK1, UK2, Yunz, Terskey ala Tau I, and Tongu-sentick glacial stage moraines were excluded because they do not follow morphostratigraphic order; most are highlighted in the original publications for the same reason. The Ghulkin II, GU3, GU4, M3, UK4, G6, BO3, and BO4 glacial stages have ages that are indistinguishable from the previous glacial advance in their respective valleys and are thus considered recessional or out of morphostratigraphic order. Moreover, these moraines were excluded in the regional age plot as they could unjustifiably create a regional stage or alter the mean age. Individual figures for excluded glacial stages are presented in Appendix D.

## 8. Discussion

We first discuss the pattern of glaciation in the Ladakh and Pangong ranges with our new  $^{10}\text{Be}$  ages and the reanalysis of ages from Owen et al. (2006) and Dortch et al. (2010a, 2011b). We then discuss regional glaciation that ranges  $>1000$  km from the northeast in the Pamir to the Puga Valley in the southwest. We conclude by discussing climatic correlation and analyze possible inheritance of  $^{10}\text{Be}$  and exhumation, toppling, and weathering of boulders and landform denudation based on the difference between our local glacial stage ages (isolated gaussians) and individual outlier ages.

### 8.1. Ladakh and Pangong ranges glaciation

Morphostratigraphically, the Indus glacial stage moraines, located on the southern slopes of the Ladakh Range, are the oldest preserved moraines in the region.

Three gaussians are apparent in the reanalysis  $^{10}\text{Be}$  ages for the Leh glacial stage for the southern slopes of the Ladakh Range. The oldest gaussian that encloses three or more ages has a peak and  $1\sigma$  of  $327 \pm 52$  ka, which agrees with the original interpretations of Owen et al. (2006) who suggested an age of MIS-6 or older. There are no correlative glacial stages in the local area.

Lateral moraines from the Deshkit-3 glacial stage are located in the northern tributaries of the Ladakh Range and can be traced into the Nubra and Shyok valleys. The more restricted Kar glacial stage advance is represented by terminal moraines in seven valleys on the southern side of the Ladakh Range. The oldest gaussians ( $\geq 3$  ages) from reanalysis of Deshkit-3 and Kar glacial stages  $^{10}\text{Be}$  ages are  $156 \pm 16$  ka and  $151 \pm 46$  ka, respectively. The Deshkit-3 age is comparable to the previously published age of  $145 \pm 12$  ka. The uncertainty of the Kar glacial stage is large due to the scatter of  $^{10}\text{Be}$  ages, which prevented Owen et al. (2006) from assigning a specific age to this glacial stage. The Deshkit-3 and Kar glacial stages ages overlap completely; thus, we suggest that they represent a synchronous glacial advance across the Ladakh Range and in the Nubra valley. There are no correlative deposits in the Pangong Range.

The Pangong-2 ( $85 \pm 15$  ka) and Ladakh-4 ( $81 \pm 20$  ka) glacial stages have nearly identical ages, which suggest synchronous glaciation in the local area. However, they overlap with reanalysis of the Bazgo glacial stage ( $60 \pm 14$  ka) located on the southern slopes of the Ladakh Range. The reanalysis of the Bazgo glacial stage is in line with Owen et al. (2006) who suggested an age of MIS 3–4.

Pangong-1 glacial stage moraines could not be dated using  $^{10}\text{Be}$  because of their poor preservation. Dortch et al. (2011b) suggest that roche moutonnées in the Tangtse Valley formed by small glaciers from the Pangong Range (Fig. 9). Reanalysis of the roche moutonnées  $^{10}\text{Be}$  ages yield a single gaussian age of  $40 \pm 3$  ka. This age is younger than the Pangong-2 ( $85 \pm 15$  ka) glacial stage and older than the Pangong cirque moraine ( $0.4 \pm 0.3$  ka). Other than the partial Pangong-1 glacial stage moraine, the roche moutonnées are the only other evidence for glaciation we found in the field. We suggest correlation of the Pangong-1 moraine remnants with roche moutonnées in the Tangtse Valley and use the roche moutonnées age ( $40 \pm 3$  ka) to define the Pangong-1 glacial stage.

Moraines from the Ladakh-2 ( $22 \pm 3$  ka) glacial stage are mapped in five of the northern valleys of the Ladakh Range. In spite of this, there are no deposits or landforms on the southern side of the range or in the Pangong Range that correlate with the Ladakh-2 glacial stage.

Reanalysis of the Khalling glacial stage, located on the southern side of the Ladakh Range, yields two gaussians, each with only two  $^{10}\text{Be}$  ages. As with Owen et al. (2006), the limited number of samples ( $n = 3$ ) prevents a definitive age, but we suggest that the older gaussian ( $15 \pm 3$  ka) with a higher peak represents the most likely age. Based on morphostratigraphy, the Khalling glacial stage on the southern side of the range should correlate with the Ladakh-1 glacial stage on the northern side of the range. Unfortunately, the Ladakh-1 glacial stage moraines were not dated; thus, this link can only be tentative.

The Ladakh Cirque ( $1.8 \pm 0.4$  ka) and Pangong Cirque ( $0.4 \pm 0.3$  ka) glacial stages moraines do not correlate with any advances in the local region. This is surprising as the wide-spread occurrence of the Ladakh and Pangong Cirque glacial stage moraines, mapped in 7 and 16 valleys, respectively, suggest that these stages should represent a strong regional signal.

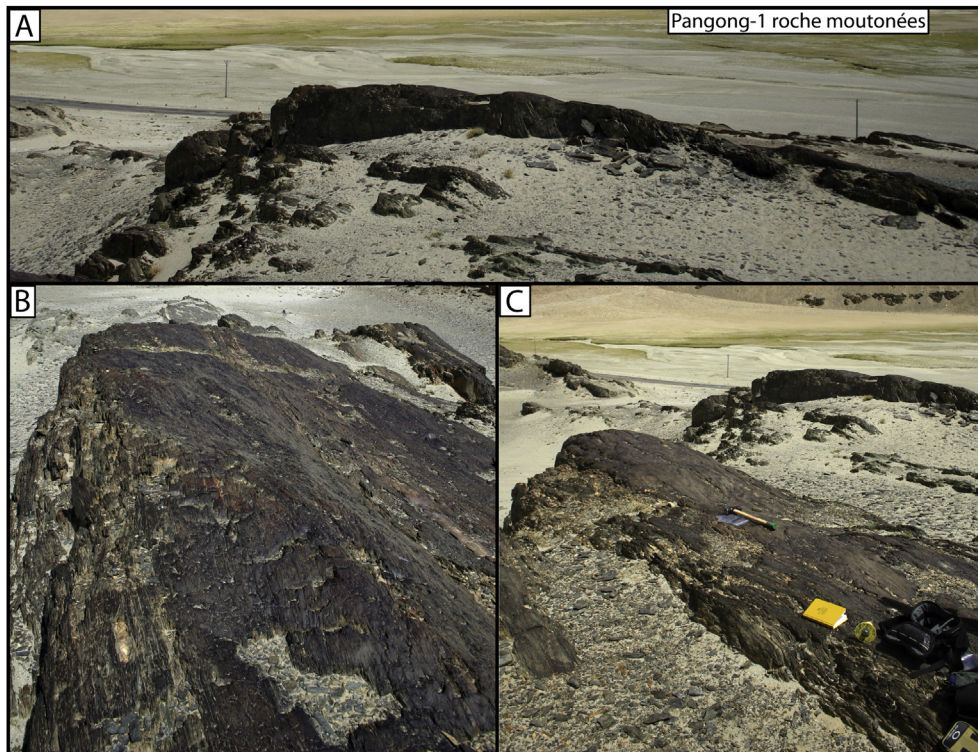


**Fig. 9.** West view of selected Pangong-1 glacial stage roche moutonnées of Dortch et al. (2011b). Roche moutonnées were draped by sand during a large flood event  $11.1 \pm 1.0$  ka. However, the whaleback shape with steep leeward (west) sides is still well preserved.

### 8.2. Asynchronous advance versus poor preservation

Many of the glacial deposits presented here do not have correlative deposits across a single range or with juxtaposed ranges (Fig. 2). Also, the extent of advance may be significantly larger on the northern side as compared with the southern side of the Ladakh Range. It seems that glaciation in these regions is asynchronous. However, several glacial stages are synchronous both across the Ladakh Range (Deshket-3 and Kar glacial stages) and between the Ladakh and Pangong ranges (Pangong-2 and Ladakh-4 glacial stages).

The question arises as to whether some glacial advances are synchronous while others are asynchronous across the region. The overall pattern of glaciation in the Ladakh Range shows restricted glaciation on the southern side with very old well-preserved deposits (Leh glacial stage), but only one glacial stage  $<60$  ka in age. On the other hand, more extensive glaciation on the northern side of the range prevented the preservation of very old deposits, but there are three sets of deposits from glacial stages  $<60$  ka in age.

We suggest that the possibility of a significant glacial advance in several valleys on only one side of a range is unlikely (e.g. the Leh and Bazgo glacial stages only occurring on the southern side and Ladakh-4 and Ladakh-2 glacial stages only occurring on the northern side of the Ladakh Range). Climatic, tectonic, and topographic forcing noted by Dortch et al. (2011a) should favor the development of glaciers and larger advances on one side (northern) of a range consistently. Switching the preferred glacier development conditions (including aspect, wind direction, orographic effect, topographic shading and higher average elevation) from southern valleys (Leh and Bazgo glacial stages) to northern valleys (Ladakh-4 and Ladakh-2 glacial stages) is highly unlikely. Synchronous advances did occur in three separate, but juxtaposed, ranges – the southern side of the Karakoram Range (Deshkit-2

glacial stage), the northern side of the Pangong Range (Pangong-2 glacial stage), and northern side Ladakh Range (Ladakh-4 glacial stage). Given these circumstances, it seems nearly impossible for a correlative advance in the southern valleys of the Ladakh Range to have not occurred.

The extent and preservation of a glacial stage may vary significantly from north to south across a single range or a region, but we argue that the timing of glaciation is generally synchronous. Many of the moraines mapped in this study are composite moraines with multiple crests, or are hummocky, which suggest incorporation of older moraines (Hambrey et al., 1997; Eyles et al., 1999). Although we only have local glacial chronologies, we nonetheless believe that in aggregate these local chronologies do represent the regional glacial history.

### 8.3. Regional glaciation

Where a significant and datable glacial advance occurs in more than one mountain range, we define a regional glacial stage as *semi-arid western Himalayan–Tibetan stage (SWHTS)* (i.e. indistinguishable ages). The SWHTS numbers (1A–9) broadly correlate with Marine Oxygen Isotope Stage (MIS) number to provide a simple naming scheme that can be changed with the addition of new data in the future. Student's *t*-test analysis of  $^{10}\text{Be}$  ages enclosed by selected gaussians reveals 16 clearly defined glacial stages ( $\geq 95\%$  confidence) and three potential regional glacial stage (Figs. 10 and 11).

Corrections for geomagnetic fluctuations have significant effect on SWHTSs 2E through 9, and subsequent correlations. Our tentative links are not only suggestive of regional climate correlations, but also point to future research. Regional glacial stages younger than SWHTS 2E are not significantly affected by geomagnetic field fluctuations and production rate uncertainties (Fig. 11). Significant

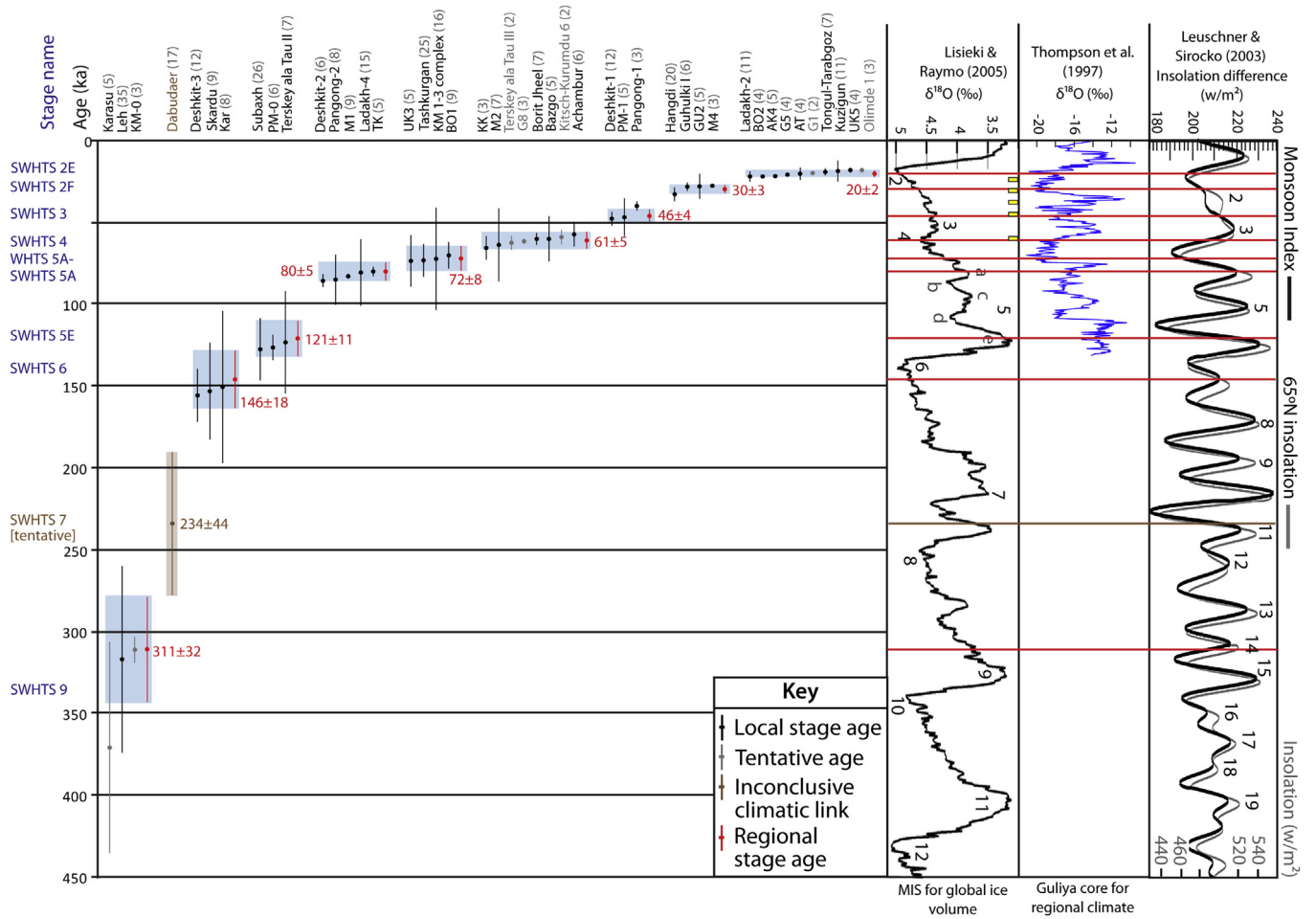


**Fig. 10.** Age plot of local glacial stages older than gLGM. Local glacial stage names are labeled in black across the top with the number of TCN samples noted in gray parentheses while regional stage ages are labeled along the Y-axes. Stacked marine  $\delta^{18}\text{O}$  curves of Lisieki and Raymo (2005), Guliya ice core  $\delta^{18}\text{O}$  record of Thompson et al. (1997), and simulated monsoon index and  $65^\circ\text{N}$  insolation of Leuschner and Sirocko (2003) are provided for comparison. Marine Oxygen Isotope Stages and monsoon peaks are labeled for reference to text. The horizontal red lines drawn over climate proxies represent the regional stage age. Heinrich events 2–6 are indicated by yellow rectangles with heights representative of 500 year uncertainty. (For interpretation of the references to color in this figure legend, the reader is referred to the web version of this article.)

correlations can be made with climate proxies. We use the Lisieki and Raymo (2005) stacking of marine  $\delta^{18}\text{O}$  records and NGRIP (2004)  $\delta^{18}\text{O}$  as a proxy for northern hemisphere events and global ice volume, Thompson et al. (1997)  $\delta^{18}\text{O}$  record of the Guliya ice core as an arid ( $\sim 200$  mm/yr precipitation) Himalaya regional glacial event proxy, and the simulated Indian monsoon index and  $\delta^{18}\text{O}$  speleothem East Asian monsoon records as proxies for precipitation activity in the orogen (Wang et al., 2001, 2008; Leuschner and Sirocko, 2003; respectively). The monsoon index is with labeled peaks corresponding to periods of strong monsoons. These proxies provide insight into the mechanisms controlling glaciation throughout the region. Proxy errors are typically  $<2\%$ , but their chronologies are determined through a number of methods including  $^{14}\text{C}$ ,  $^{36}\text{Cl}$ ,  $^{230}\text{Th}$ , and orbital tuning. Therefore, we refer the reader to the original publications for information about the quality and associated errors of each proxy (Thompson et al., 1997; Wang et al., 2001, 2008; Leuschner and Sirocko, 2003; NGRIP, 2004; Lisieki and Raymo, 2005). Each glacial stage is discussed in chronological order below.

### 8.3.1. Oldest glacial stage/s

Evidence for old glaciations has been recognized in the western Himalaya and includes the Bunthang, Deshkit-4, and Indus glacial

stages (Owen et al., 2006; Seong et al., 2007; Dortch et al., 2010a). Based on paleomagnetic methods, Cronin et al. (1989) defined the Bunthang glacial stage as  $\geq 720$  ka. The Deshkit-4 glacial stage remains undefined because the landform and boulders were too degraded. Boulder ages from the Indus glacial stage moraines are younger than indicated by morphostratigraphy, but an alluvial fan that overlies the moraines was dated using a  $^{10}\text{Be}$  depth profile at 430 ka, which places a minimum age on Indus glacial stage (Owen et al., 2006). It is not possible to determine whether the Bunthang, Deshkit-4, and Indus glacial stages were synchronous, but based on morphostratigraphy and regional correlation, they are all older than MIS 9.

### 8.3.2. SWHTS 9

Very few samples were collected from the highly degraded Karasu ( $n = 5$ ) and KM-0 ( $n = 3$ ) glacial stage moraines, located in the Karakoram and Zaskar, respectively (Seong et al., 2009a,b,c; Hedrick et al., 2011). The oldest gaussians in both chronologies only contains two ages so a definitive age cannot be assigned. However, we do report tentative ages (Fig. 10) of  $371 \pm 65$  ka for Karasu glacial stage and  $311 \pm 8$  ka for KM-0 glacial stage. These tentative ages correlate with the Leh glacial stage ( $317 \pm 57$  ka) on the southern flank of the Ladakh range. We argue that the robust

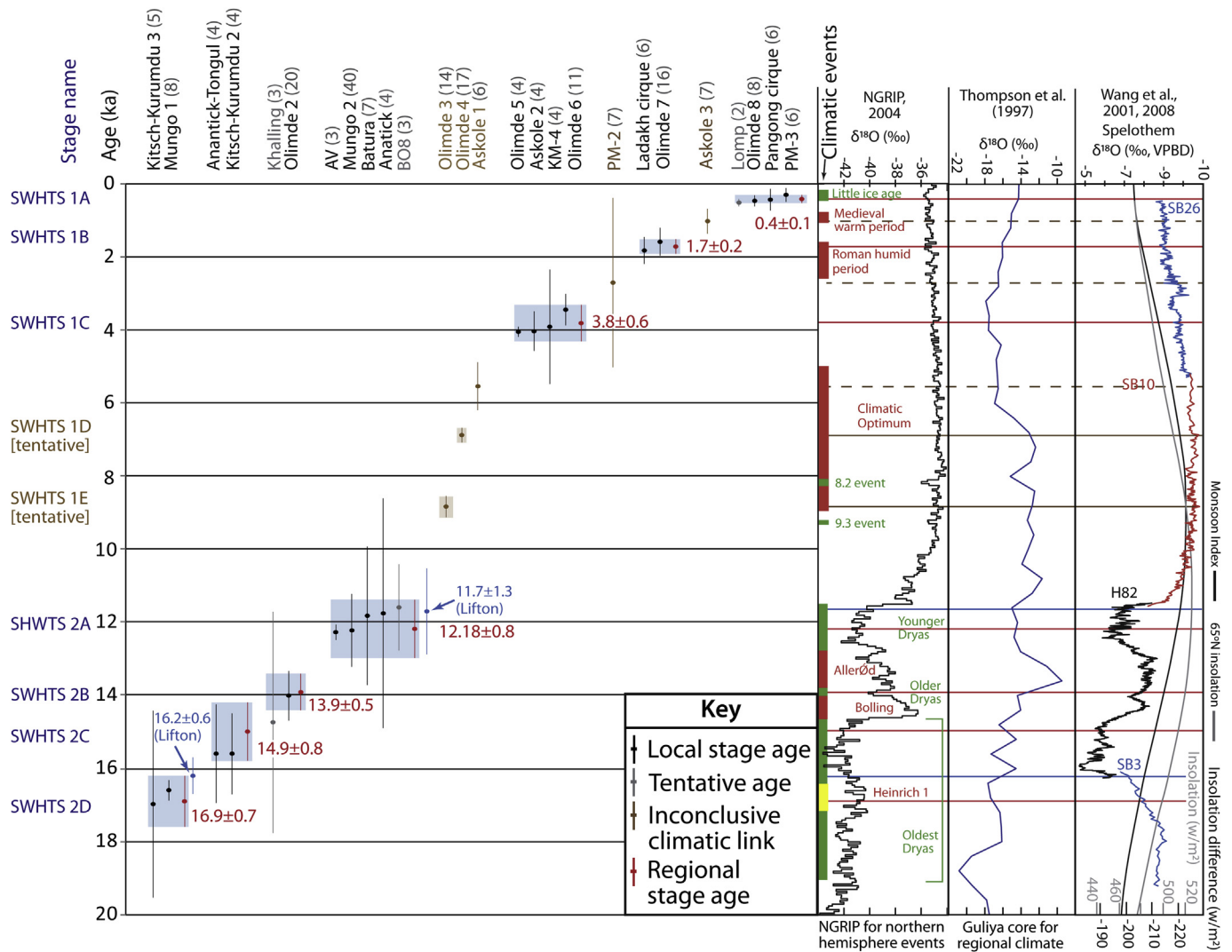


**Fig. 11.** Age plot of local glacial stages gLGM and younger. Local glacial stage names are labeled in black across the top with the number of TCN samples noted in gray parentheses while regional stage ages are labeled along the Y-axes. Blue markers denote the regional stage ages of SWHTS 2a and 2c if geomagnetic corrections of Lifton et al. (2005) are used. NGRIP (2004)  $\delta^{18}\text{O}$  curve, Guliya ice core  $\delta^{18}\text{O}$  record of Thompson et al. (1997), Wang et al. (2001, 2008) Chinese speleothem  $\delta^{18}\text{O}$  curve, and simulated monsoon index and  $65^\circ\text{N}$  insolation of Leuschner and Sirocko (2003) are provided for comparison. The duration of specific climatic events are marked by red, green, and yellow vertical rectangles. The horizontal red lines drawn over climate proxies represent the regional stage age. Heinrich event 1 is indicated by yellow rectangles with heights representative of 500 year uncertainty. (For interpretation of the references to color in this figure legend, the reader is referred to the web version of this article.)

chronology for the Leh glacial stage and the tentative ages of the Karasu and KM-0 glacial stages justifies the delineation SWHTS 9. The mean and MAD of SWHTS 9 is  $311 \pm 32$  ka.

The large uncertainty associated with SWHTS 9 precludes any meaningful correlation with climate records. SWHTS 9 may be linked to MIS 9/10, or the local glacial stages independently linked to monsoon peaks 14, 15, and 17. Further dating of suitably old glacial debris will help to clearly define this regional glacial stage in the future. Adding more ages will make Student's *t*-test more robust and lower the MAD leading to clearer definition of regional glacial stage limits.

### 8.3.3. SWHTS 7 [tentative]

The Dabudaer glacial stage, which comprises moraines in three valleys in the southeast Pamir, has a gaussian age of  $234 \pm 44$  ka. Owen et al. (2012) dated 17 boulders and the oldest gaussian encloses four ages. This stage was mapped in and dated from three tributary valleys to the Tashkurgan Valley. Thus, we suggest a

tentative SWHTS 7 regional stage (Fig. 10). The large error of SWHTS 7 makes it difficult to correlate with climate records.

### 8.3.4. SWHTS 6

The selected gaussians for the Deshkit-3 ( $156 \pm 16$  ka), Skardu ( $153 \pm 30$  ka), and Kar ( $151 \pm 46$  ka) glacial stages cluster well. However, their spatial occurrence is restricted to the northern and southwestern ends of the study region (Fig. 12). The mean and MAD of  $^{10}\text{Be}$  ages defines SWHTS 6 at  $146 \pm 18$  ka (Fig. 10). SWHTS 6 is centered on a moderate monsoon peak (7) during the cold period and high global ice volume of MIS-6. This suggests that glaciers reached their maximum extent with increased monsoon precipitation and that these glaciers also responded to lower temperatures.

### 8.3.5. SWHTS 5E

The ages from the Subaxh ( $128 \pm 19$  ka), PM-0 ( $126 \pm 8$  ka), and Terskey ala Tau II ( $123 \pm 31$  ka) glacial stages have a mean and MAD

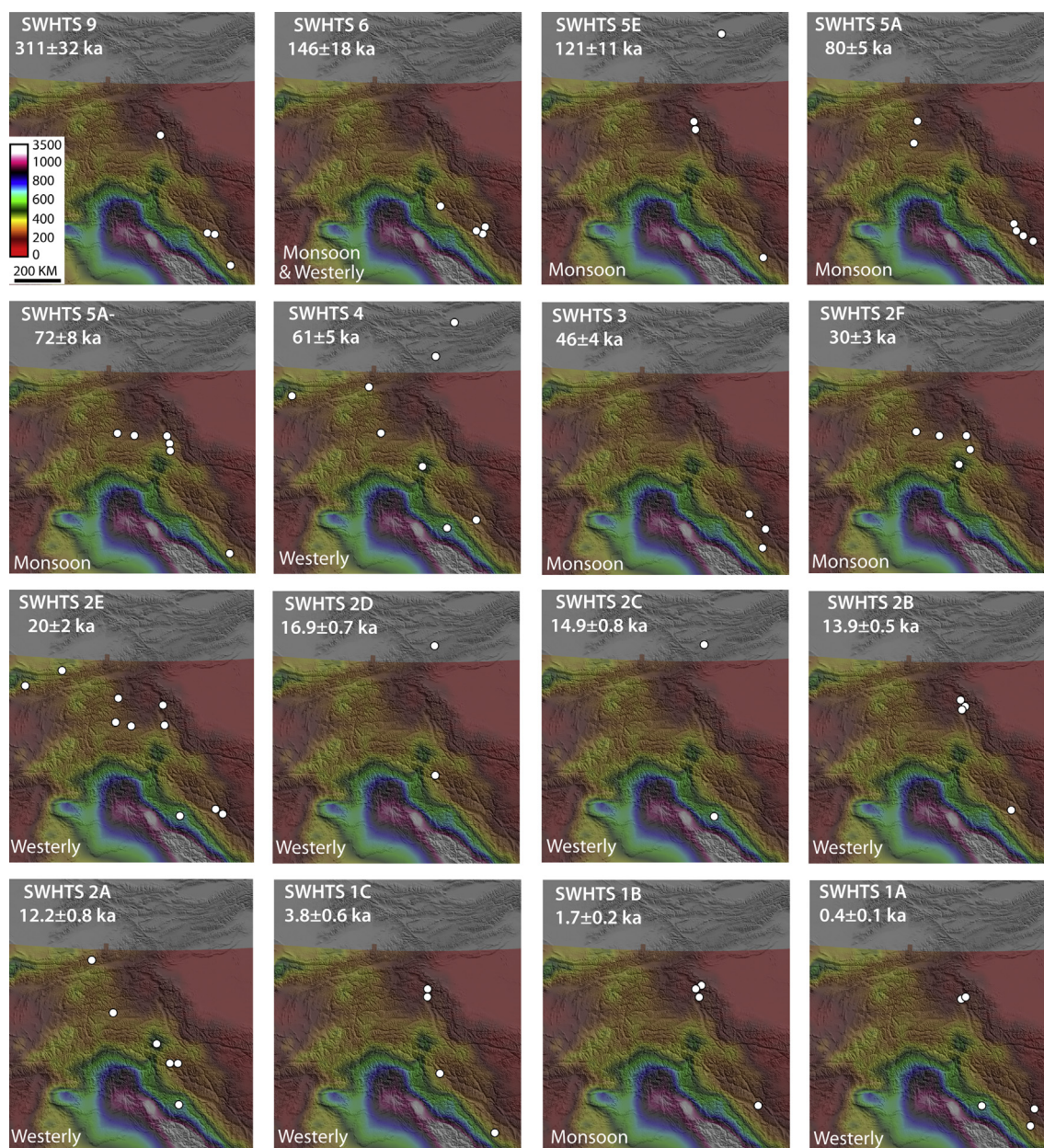


**Fig. 12.** SRTM hillshade DEMs of the study area (see Fig. 1 for location) with semi-transparent TRMM imagery from 1998 to 2008 (Bookhagen and Burbank, 2006; Bookhagen, 2013) for each regional glacial stage. Local glacial stage locations marked by white dots and suggested climatic driver labeled in bottom left corner. Tentative stages SWHTS 7, 1E, and 1D are not shown because their single range occurrence results in no observable regional spatial distribution.

of  $121 \pm 11$  ka and cover three separate mountain ranges. Spatial occurrence of glaciation during this time is restricted to the eastern half of the study area (Fig. 12). SWHTS 5E is centered on MIS-5e just after monsoon peak 6, which suggest that these glaciers are more sensitive to monsoon precipitation and less sensitive temperature as compared to the areas affected by SWHTS 6.

### 8.3.6. SWHTS 5A

The selected gaussians of the Dshkit-2 ( $86 \pm 4$  ka), Pangong-2 ( $85 \pm 15$  ka), M1 ( $84 \pm 1$  ka), Ladakh-4 ( $81 \pm 20$  ka), and TK ( $80 \pm 3$  ka) local glacial stages cover two mountain ranges in the northwest and 3 ranges in the southeast of the study area (Figs. 10 and 12). The combined  $^{10}\text{Be}$  data yields an age of  $80 \pm 7$  ka.

SWHTS 5A occurs during interstadial MIS 5a, a moderate negative  $\delta^{18}\text{O}$  depression in the Guliya ice core, and monsoon peak 4. The increase in monsoon strength leading up to peak 4 likely

supplied more moisture to glaciers leading to advance and maximum extent during the moderate glacial shown by the Guliya record. The decrease in monsoon strength immediately after MIS 5a likely led to the termination of the regional glacial stage. We argue that SWHTS 5A glaciation is controlled by monsoon precipitation and that these glaciers are more sensitive to precipitation than cold temperatures.

### 8.3.7. SWHTS 5A-

The selected gaussians of the UK3 ( $73 \pm 16$  ka), Tashkurgan ( $73 \pm 10$  ka), KM 1–3 complex ( $72 \pm 31$  ka), and BO1 ( $70 \pm 8$  ka) local glacial stages cluster exceptionally well even though scatter in individual local stage  $^{10}\text{Be}$  ages create large uncertainties. Analysis of the combined  $^{10}\text{Be}$  ages using Student's *t*-test shows that SWHTS 5A- is distinctly different from SWHTS 5B or SWHTS 4 at the 99% confidence level despite the overlap in uncertainties. The combined

$^{10}\text{Be}$  ages have a mean age and MAD of  $72 \pm 8$  ka, and cover three ranges in the center and one range in the southeast of the study area (Figs. 10 and 12).

Termination of this glacial stage occurred, most notably, after a sharp decrease in  $\delta^{18}\text{O}$  in the Guliya ice core record; just after a small peak following MIS-5A where mid-latitude westerlies are strengthening. This suggests that maximum glacier extent occurred during the Guliya interstadial and small peak following MIS-5A due to monsoon precipitation and that this event was out of phase with both proxy records. However, monsoon intensity was also in decline. Thus, we argue that SWHTS 5A- represents a selection of glaciers that are very sensitive to moisture and maintained their maximum position from MIS-5A until immediately after the Guliya interstadial and short marine  $\delta^{18}\text{O}$  excursion (post MIS-5A) when climatic conditions (declining monsoon intensity) became too unfavorable.

#### 8.3.8. SWHTS 4

Only two samples were collected from the Terskey ala tau III and Kitsch-Kurumdu 6 local glacial stages; however they have a normal distribution. Thus, we provide tentative ages of  $62 \pm 4$  ka and  $59 \pm 5$  ka, respectively. Three samples were collected from the G8 glacial stage but the distribution is bi-modal. Thus, we take the oldest-highest probability gaussian with two ages to define a tentative stage age of  $62 \pm 2$  ka.

The selected gaussians for the KK ( $66 \pm 7$  ka), M2 ( $64 \pm 22$  ka), Terskey ala tau III ( $62 \pm 4$  ka), G8 ( $62 \pm 2$  ka), Borit Jheel ( $60 \pm 4$  ka), Bazgo ( $60 \pm 14$  ka), Kitsch-Kurumdu 6 ( $59 \pm 5$  ka), Achanbur ( $57 \pm 7$  ka) local glacial stages cluster together well, and cover eight ranges across the entire study area (Figs. 10 and 12). The combined  $^{10}\text{Be}$  ages result in a regional stage age and MAD of  $61 \pm 5$  ka.

SWHTS 4 terminated during the cold trough of MIS 4, synchronous with the end of a Guliya ice cap glacial, and midway up towards monsoon peak 3. The strengthening of the monsoon and the weakening influence of the mid-latitude westerlies likely terminated this glacial stage; thus, we suggest cold temperatures and precipitation from the mid-latitude westerlies forced glaciation.

#### 8.3.9. SWHTS 3

The selected gaussians for the Deshkit-1 ( $48 \pm 4$  ka), PM-1 ( $47 \pm 22$  ka), and Pangong-1 ( $40 \pm 3$  ka) glacial stages cluster well, and the combined  $^{10}\text{Be}$  ages define the regional stage age at  $46 \pm 4$  ka. The spatial distribution for dated glacial sediments are confined to the southwestern end of the study area (Figs. 10 and 12), but span three separate ranges (Karakorum, Ladakh, and Zaskar ranges).

SWHTS 3 terminates during a relatively cold period (MIS-3), synchronous with the end of a Guliya ice cap glacial, and immediately after a decline in monsoon strength (monsoon peak 3). We suggest glaciers reached their maximum extent during the peak of MIS 3 and monsoon peak 3, out of phase with the Guliya ice cap  $\delta^{18}\text{O}$  record, and that this glacial stage was dominantly controlled by the monsoon driving precipitation sensitive glaciers.

#### 8.3.10. SWHTS 2F

The selected gaussians for the Hangdi ( $33 \pm 4$  ka), Ghulkin I ( $28 \pm 3$  ka), GU2 ( $28 \pm 8$  ka), and M4 ( $28 \pm 0.3$  ka) local glacial stages cluster well, occupy four separate ranges, and combined  $^{10}\text{Be}$  ages have a mean age and MAD of  $30 \pm 3$  ka. The spatial distribution of dated preserved deposits is confined to the center of the study area (Figs. 10 and 12).

SWHTS 2F deglaciation occurs in the beginning of cold MIS 2, synchronous with Guliya ice core  $\delta^{18}\text{O}$  depression, and during a decline in monsoon strength similar to SWHTS 3. The decrease in precipitation from weakening of the monsoon likely terminated

glacier advance. Thus, glaciers would have likely reached their maximum positions during monsoon/insolation peak 2.

#### 8.3.11. SWHTS 2E

Only two samples were collected from the G1 glacial stage; however they provide a normal fit and a tentative age of  $20 \pm 0.3$  ka. Two gaussians were separated from the Olimde-1 glacial stage cumulative PDF, but because only three samples were collected, neither gaussian meets our criteria. We use the gaussian at  $17.5 \pm 0.7$  ka that encloses 2 ages with the highest probability as a tentative age.

The selected gaussians for the Ladakh-2 ( $22 \pm 3$  ka), BO2 ( $22 \pm 0.3$  ka), AK4 ( $22 \pm 1$  ka), G5 ( $21 \pm 0.8$  ka), AT ( $20 \pm 4$  ka), G1 ( $20 \pm 0.3$  ka), Tarangoz Tongul ( $19 \pm 2$  ka), Kuzigun ( $19 \pm 6$  ka); UK5 ( $18 \pm 1$  ka), and Olimde-1 ( $18 \pm 1$  ka), glacial stages cluster well, and have combined  $^{10}\text{Be}$  ages with a mean and MAD of  $20 \pm 2$  ka (Fig. 10). This has excellent correlation with the LGM ( $21 \pm 2$  ka) as defined by Mix et al. (2001). Moreover, our regional stage age ( $20 \pm 2$  ka) overlaps with the identified LGM signal from the Guliya ice core signified by a sharp  $\delta^{18}\text{O}$  depression at  $18 \pm 1$  ka (inferred age; Thompson et al., 1997). Spatial distribution of local glacial stages covers ten ranges across the entire study area except for the Tien Shan (Fig. 12). Although this regional stage has more individual occurrences, SWHTS 4 has a larger overall spatial distribution.

SWHTS 2E deglaciation occurs just before the stacked  $\delta^{18}\text{O}$  ocean records maximum and Guliya ice core minimum, and just past the monsoon index minimum. In spite of decreasing temperatures toward MIS-2  $\delta^{18}\text{O}$  maximum, the increase in monsoon influence and weakening of the mid-latitude westerlies likely terminated this glacial stage. We suggest that these glaciers were fed by mid-latitude westerlies precipitation.

#### 8.3.12. SWHTS 2D

The highest probability gaussian for the Kitsch-Kurumdu 3 glacial stage encloses 4 ages and has a peak and sigma of  $17.0 \pm 2.6$ . The Mungo-1 glacial stage ( $16.9 \pm 0.7$  ka) is clearly defined by the tight clustering of six ages. The mean age and MAD of the combined  $^{10}\text{Be}$  ages is  $16.8 \pm 0.4$  ka, designated as SWHTS 2D (Fig. 11). Spatial distribution of glaciation is limited to the far north and south of the study area. The poor distribution is likely due to the paucity of sediments dated to this time period (Fig. 12).

SWHTS 2D correlates with the Oldest Dryas and Heinrich event-1. This indicates termination of this glacial stage was synchronous with northern hemisphere climatic changes, and was likely controlled by precipitation from the mid-latitude westerlies.

Fluctuations in the geomagnetic field have little effect on the mean age of this glacial stage and our correlations. For example, the most disparate difference is caused by the corrections in the Lifton et al. (2005) scheme, which results in a mean age of  $16.2 \pm 0.6$  ka (Fig. 11). The  $\sim 700$  year difference is within uncertainty of our preferred time-independent Lal (1991) and Stone (2000) scheme.

#### 8.3.13. SWHTS 2C

Only one gaussian encloses  $\geq 3$  ages was separated from both the Anantick-Tongul and Kitsch-Kurumdu 2 local glacial stage cumulative PDFs. The resulting stages are defined at  $15.6 \pm 1.4$  ka and  $15.6 \pm 1.1$  ka, respectively. The mean age and MAD of the combined  $^{10}\text{Be}$  ages is  $14.9 \pm 0.8$  ka, designated as SWHTS 2C (Fig. 11). Similar to SWHTS 2D, the spatial distribution of glaciation is limited to the far north and south of the study area and poor distribution is likely due to the paucity of sediments dated to this time period (Fig. 12). Comparison of this stage with SWHTS 4 yields a  $p$ -value of 0.04, which indicates that the distribution of exposure ages are distinct at  $>95\%$  confidence level.

SWHTS 2C terminates at the end of the oldest Dryas event just before the increase in temperatures at the Bolling transition as recorded in both the NGRIP and speleothem  $\delta^{18}\text{O}$  records (Wang et al., 2001, 2008; NGRIP, 2004). The 400 year  $\delta^{18}\text{O}$  sampling averages from the Guliya ice core yield a low-resolution record that is difficult to make specific comparisons with on the <21 ka timescale.

#### 8.3.14. SWHTS 2B

Two gaussians were separated from the Khalling glacial stage, but because only three samples were collected, neither gaussian meets our criteria. We use the gaussian at  $14.7 \pm 3.0$  ka that encloses 2 ages with highest probability as a tentative age. In contrast, the Olimde-2 event clusters well with the highest probability gaussian enclosing 13  $^{10}\text{Be}$  ages at  $14.0 \pm 0.7$  ka. Spatial distribution is limited to the eastern, more arid, portion of the study area. The combined  $^{10}\text{Be}$  ages have a mean age and MAD of  $13.9 \pm 0.5$  ka and are centered on the Older Dryas (Fig. 11). Due to the age uncertainty, we can only tentatively link SWHTS 2B to the older Dryas, northern hemisphere oscillations, and the mid-latitude westerlies.

#### 8.3.15. SWHTS 2A

The selected gaussians for the AV ( $12.3 \pm 0.3$  ka), Mungo-2 ( $12.2 \pm 1.0$  ka), Batura ( $11.8 \pm 1.9$  ka), Ananick ( $11.8 \pm 3.2$  ka), BO8 ( $11.6 \pm 1.2$  ka) glacial stages cluster well despite scatter of individual ages within each selected gaussian. Spatial distribution confined to the central and southeastern portions of the study area (Figs. 11 and 12). The combined  $^{10}\text{Be}$  ages have a mean age and MAD of  $12.22 \pm 0.76$  ka (Lal, 1991; Stone, 2000);  $11.71 \pm 1.27$  ka using the methods of Lifton et al. (2005). The small difference of 0.51 ka (510 years) lends confidence to correlation with the Younger Dryas events recorded in both NGRIP and speleothem  $\delta^{18}\text{O}$  records (Wang et al., 2001, 2008; NGRIP, 2004), northern hemisphere climatic oscillations, and the mid-latitude westerlies. Since geomagnetic correction has less effect on younger glacial stages, we do not discuss their effect beyond this point. We term this regional glacial stage SWHTS 2A, which has an age and MAD of  $12.2 \pm 0.2$  ka.

#### 8.3.16. SWHTS 1E and SWHTS 1D [tentative]

The Olimde-3 ( $8.3 \pm 0.3$  ka) and Olimde-4 ( $6.9 \pm 0.2$  ka) glacial stages have well defined gaussians PDFs with >3 ages. Regional glacial stages cannot be definitively defined by our criteria as they only occur within a single mountain range. However, each local stage occurs and has been dated within multiple valleys. Moreover, there is a notable lack of focus on Holocene glacial sediments and landforms dated within the cosmogenic dating community within the Himalaya–Tibetan orogen (Owen et al., 2008). Therefore, the lack of other sediments dated to these ages is likely the result of a paucity of studies. Thus, we suggest two tentative regional stages; SWHTS 1E at  $8.3 \pm 0.3$  ka and SWHTS 1D at  $6.9 \pm 0.2$  ka.

We refrain from making concrete climatic correlations with SWHTS 1E and SWHTS 1D tentative stages. However, we speculate that both stages potentially correlate with the climatic optimum and, more tantalizingly, the two most negative peaks in the  $\delta^{18}\text{O}$  speleothem records of Wang et al. (2001, 2008). This suggests that these seemingly isolated advances on massifs surrounded by low-relief topography could be controlled by East Asian monsoon moisture, and are more sensitive to precipitation than temperature. However, using palynology and radiocarbon methods, Demske et al. (2009) suggests increasing westerly influence and precipitation between 9.2 and 4.8 ka BP. Future work focused on post gLGM deposits will likely define one or more glacial stages between 4 and 11 ka, potentially with interesting climatic consequences.

#### 8.3.17. Undefined events

The Askole-1 ( $5.5 \pm 0.6$  ka) glacial stage has well defined gaussian with >3 ages. We cannot define a definitive regional glacial stage because the Askole-1 local glacial stage has only been dated in one valley in one mountain range. Future work focused on Holocene glaciation in the region may reveal similar aged deposits.

#### 8.3.18. SWHTS 1C

Selected gaussians for the Olimde-5 ( $4.0 \pm 0.1$  ka), Askole-2 ( $4.0 \pm 0.5$  ka), KM-4 ( $3.9 \pm 1.6$  ka), and Olimde-6 ( $3.4 \pm 0.4$  ka) glacial stages cluster well and cover three mountain ranges that are spread evenly across the region of study (Figs. 11 and 12). The combined  $^{10}\text{Be}$  ages define SWHTS 1C at  $3.8 \pm 0.6$  ka.

SWHTS 1C does not correlate with any specific climatic event. Broadly, the glacial stage is coincident with decreasing monsoon influence between marked warm events equivalent to the Little Climatic Optimum and the Roman Humid period. The decreasing monsoon influence and the occurrence between warm periods suggest that SWHTS 1C is tied to northern hemisphere oscillations with dominant moisture supply brought via the mid-latitude westerlies.

#### 8.3.19. Undefined event

The large error of the PM-2 local glacial stage ( $2.7 \pm 2.3$  ka) prevents conclusive correlation with any regional glacial stage of specific climatic events (SWHTS 1C [ $p$ -value = 0.28] and SWHTS 1B [ $p$ -value = 0.21]; Fig. 11). Grouping PM-2 with SWHTS 1C or 1B has no observable effect on the mean and MAD of the combined  $^{10}\text{Be}$  ages of the regional stages. Moreover, excluding PM-2, Student's- $t$  test shows that SWHTS 1C and 1B are distinct ( $p$ -value = 0.00). PM-2 local glacial stage is only included here for completeness.

#### 8.3.20. SWHTS 1B

Selected gaussians for the Ladakh Cirque ( $1.8 \pm 0.4$  ka) and Olimde-7 ( $1.6 \pm 0.4$  ka) glacial stages cluster well and occur in two mountain ranges in the middle and south eastern portions of the region of study (Figs. 11 and 12). The combined  $^{10}\text{Be}$  ages define SWHTS 1B at  $1.7 \pm 0.2$  ka.

SWHTS 1B termination correlates with the end of the Roman humid period, just after an increase in the  $\delta^{18}\text{O}$  speleothem records of Wang et al. (2001, 2008). However, enhanced Indian monsoon precipitation is recorded near the southern site of glaciation between 2.1 and 3.4 ka in  $\delta^{18}\text{O}$  concentrations in lacustrine sediments from Pangong Tso (Gasse et al., 1996). We suggest that Indian monsoon precipitation drove glaciation to its maximum extent for SWHTS 1B. The decrease in monsoon precipitation after 2.1 ka likely led to moraine abandonment and subsequent stabilization by 1.7 ka.

#### 8.3.21. Undefined event

Analysis of the Askole-3 ( $1.0 \pm 0.3$  ka) local glacial stage using Student's  $t$ -test shows that it is distinct from SWHTS 1B and SWHTS 1A. As of now, it is an isolated event, dated in one valley in one mountain range, which does not justify the designation of a regional glacial stage based on our criteria. It does correlate with the medieval warm period, suggesting that advance was tied to monsoon precipitation. However, the paucity of other glacial sediments dated to this time makes these linkages speculative.

#### 8.3.22. SWHTS 1A

Selected gaussians for the Lomp ( $0.5 \pm 0.1$  ka), Olimde-8 ( $0.5 \pm 0.2$  ka), Pangong Cirque ( $0.4 \pm 0.3$  ka), and PM-3 ( $0.3 \pm 0.2$  ka) glacial stages cluster well. Spatial distribution is spread across the central and southeastern portions of the study area (Figs. 11 and 12), which is most likely due to the paucity of studies focused on post LGM glaciation in this region.

The combined  $^{10}\text{Be}$  ages define SWHTS 1A at  $0.4 \pm 0.1$  ka, which overlaps the first half of the Little Ice Age (Grove, 2004). SWHTS 1A occurred during a time of decreased monsoon influence and is correlative with changes in northern hemisphere climate. Precipitation for glacier advance would have been brought by the mid-latitude westerlies.

#### 8.4. Regional glaciation and climate

Broadly, our results suggest that the more extensive late Pleistocene glaciations are associated with the monsoon, while smaller (post) gLGM glaciations are associated with the mid-latitude westerlies. Most (6 of 7 or 86%) of the regional glacial stages between SWHTS 6 (146 ka) and SWHTS 2E (30 ka) are associated with monsoon peaks. In contrast (7 of 8 or 88%) of regional glacial stages between SWHTS 2E (20 ka) though SWHTS 1A (0.4 ka) are linked to cold events in the Northern Hemisphere, possibly teleconnected by the mid-latitude westerlies (Fig. 12). Tentative stages SWHTS 7, 1E, and 1D are not included here due to uncertainty of regional representation. One hypothesis is that the monsoon has become less dominant during the Last Glacial cycle ( $\leq 21$  ka). However, we do not favor this explanation as early- and mid-Holocene advances linked to monsoons have been shown in other areas throughout the Himalayan Tibetan plateau (c.f. Owen, 2009). Instead, we speculate that glacial advances driven by the mid-latitude westerlies, in general, have a smaller extent compared to monsoon driven advance. The paucity of older glacial sediments that correlate to cold Northern Hemisphere oscillations is due to lack of preservation (i.e. more extensive subsequent monsoon driven glaciation would destroy debris from the less extensive westerly driven glacial advances). If true, the Indian monsoon is the primary shaper of topography in this region with significant influence over glaciation, mass movements, and fluvial systems (Bookhagen et al., 2005; Dortch et al., 2009, 2011a,b; Bookhagen, 2013).

There is clear synchronicity across the region regardless of suggested mid-latitude westerlies or monsoon dominance, geographic location, or modern climate (Fig. 12). For example, stages SWHTS 2A, 2B, 2C and 2D correlate with Northern Hemisphere cold periods (Younger Dryas, Older Dryas [tentative], Oldest Dryas) where the influence of the mid-latitude westerlies would have greater influence teleconnecting into mid- and high-latitude North Hemisphere climate systems (Fig. 11). The mid-latitude westerlies would enable transport of significant moisture to the Himalaya causing glaciers to advance. Termination of SWHTS 4 ( $61 \pm 5$  ka) correlates with Heinrich event-6 ( $60 \pm 0.5$  ka), SWHTS 3 ( $46 \pm 4$  ka) with Heinrich event-5 ( $45 \pm 0.5$  ka), SWHTS 2F ( $30 \pm 3$  ka) with Heinrich event-3 ( $31 \pm 0.5$  ka), and SWHTS 2C with ( $17.0 \pm 0.6$  ka) with Heinrich event-1 ( $16.8 \pm 0.5$  ka; Hemming, 2004). Heinrich events are plotted as yellow rectangles, with 500-year uncertainty (height of rectangle) as suggested by Hemming (2004), in Figs. 10 and 11. A specific connection between glaciation termination and every other Heinrich event cannot yet be established, but the correlation does indicate an in phase connection between Himalayan glaciation and Northern Hemisphere climate. Future studies may find linkages with cooler sea surface temperatures and limited ability of the mid-latitude westerlies to pick up moisture or a shift in the Inter Tropical Convergence Zone.

We have identified 16 regional stages, many of which occurred in short temporal succession, that are statistically distinct and separate. Moreover, all of the proxies in this study point to numerous glacial cycles, something that is rarely observable in the record of terrestrial glacial sediments due to poor preservation. We conclude that glaciers respond to both mid-latitude westerlies and monsoon influence, but that in general, more extensive advances occur due to the influence of monsoons. Broadly, the dominance of

climatic systems during glacial periods can change with timescale; pre-gLGM glaciation is monsoon controlled while post-gLGM glaciation is westerly controlled. Post-gLGM glacial debris will likely be obliterated by the next extensive monsoon driven glaciation. Moreover, the presence of regional synchronicity suggests that the pattern of spatial distribution likely has more to do with: 1) location of studies; and 2) individual glaciers sensitivity to temperature or precipitation rather than the source of moisture supply.

#### 8.5. The young, the old, and the ugly

This regional synthesis has recalculated and analyzed 692  $^{10}\text{Be}$  ages. Of these, regional glacial stages were determined from the distribution of 353 ages, 192 were excluded as young outliers, 50 were excluded as old outliers, and 97 either failed to cluster or were redundant. In section 8.5.1 and 8.5.2, we examined the young and old outliers respectively and conclude with a short summary.

##### 8.5.1. Too young

Exposure dating can yield ages that are too young due to chemical and physical boulder surface weathering (spalling, salt-crystal and clay wedging of grains, frost shattering, etc.), boulder exhumation, boulder toppling, and moraine degradation (slope and freeze-thaw processes, soil erosion, etc.). These processes have been examined specifically in Putkonen and Swanson (2003), Zech et al. (2005b), Putkonen and O'Neal (2006), Seong et al. (2009d), and Heyman et al. (2011). These processes are not covered in detail here as we cannot distinguish between the various processes by examining the distribution of outliers, that is, loss of a thick spall would result in an exposure age indistinguishable from a recently exhumed boulder.

Analysis of outliers is limited to the datasets used to define local and regional glacial stages (i.e. 595 of 692). In this study we isolated 155 of 321  $^{10}\text{Be}$  ages from landforms older than the gLGM and 37 of 274 ages from landforms gLGM and younger in age (see plots in Appendix B and C for outliers). These outliers were plotted against the originating local glacial stage gaussian ages in both age and percent.

Pre-gLGM age underestimation is more than thrice as common (48.3% vs. 13.5%) compared to deposits younger than the gLGM. However, the significance is similar, as demonstrated by Fig. 13A, which clearly shows no correlation between the percentages of age underestimation compared to selected gaussian ages (LGM plotted as blue dashed line). This is surprising as there is a strong positive correlation ( $r^2 = 0.86$ ) between the degree of under exposure in (ka) and gaussian age (Fig. 13B). Overall, under exposure averages  $\sim 45\%$  across all timescales (Fig. 13C).

Small amounts of under exposure are difficult to isolate among old and scattered  $^{10}\text{Be}$  ages, thus the average amount of under exposure is artificially increased while the occurrence is artificially decreased. We suggest that under exposure affects  $>48.3\%$  of dated pre-gLGM boulders. Our method may be insensitive to a  $\sim 6\%$  age underestimation on all time-scales. This is explicitly shown in Fig. 13C where numerous outliers are present near the green-dashed 1:1 line. However, more datasets will need to be analyzed to confirm this point.

##### 8.5.2. Too old

Identifying and correcting for inherited debris is important. There are three general modes of incorporating material with inherited  $^{10}\text{Be}$ : *in situ* prior exposure, prior exposure during transport, and prior exposure due to reworking.

*In situ* prior exposure, where  $^{10}\text{Be}$  are accumulated in bedrock before removal by a glacier, can significantly affect both young and old deposits. Young and presumably less extensive deposits are

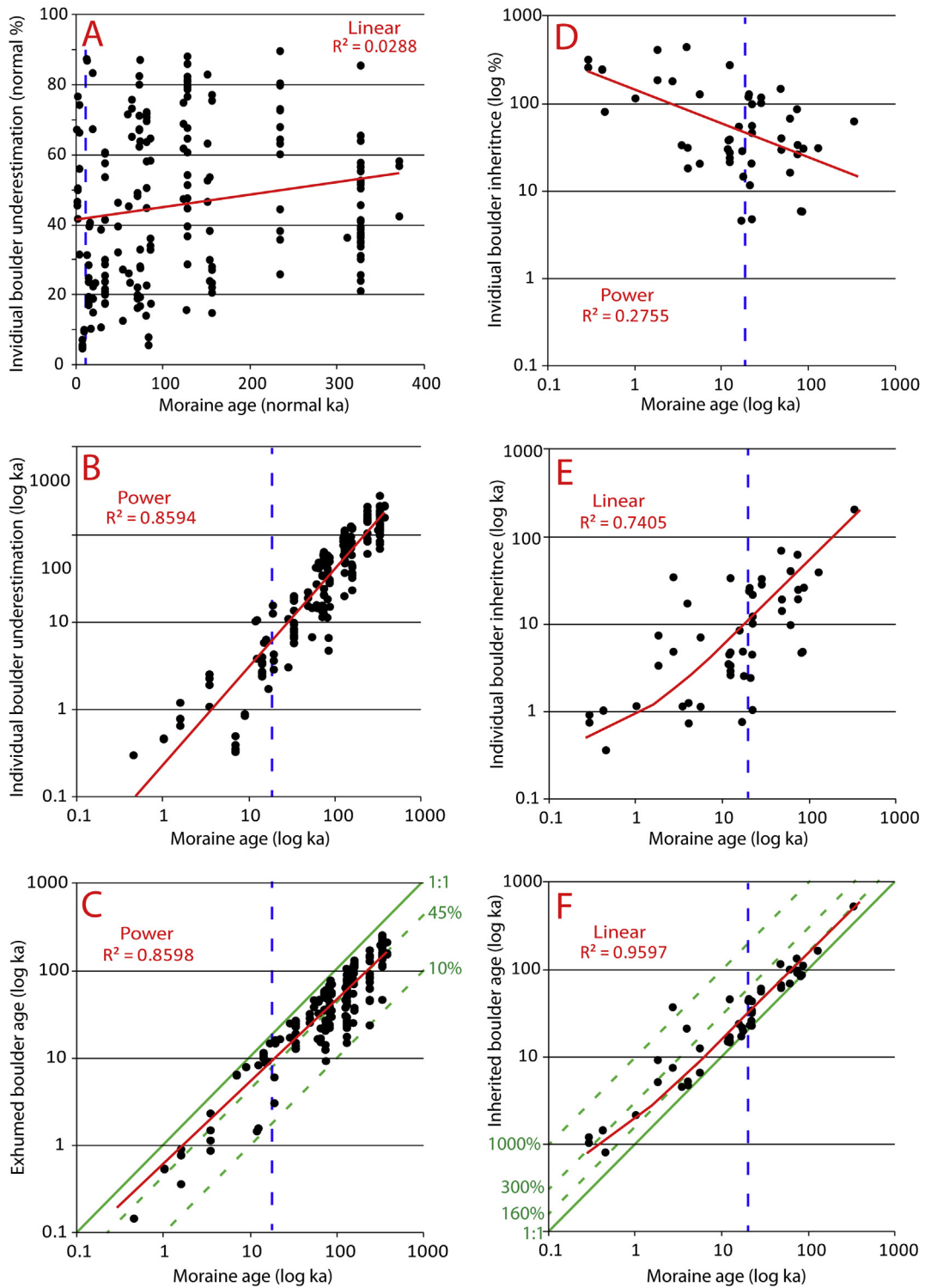


**Fig. 13.** Plot of all outliers (192 underestimated and 50 inherited) vs. respective gaussian age. (A) Normal plot of age underestimation as percent of gaussian age versus gaussian age. (B) Log–log plot of age underestimation in ka versus gaussian age. (C) Log–log plot of underestimated outlier boulder ages versus gaussian age. (D) log–log plot of boulder inheritance as percent of gaussian age versus gaussian [boulder at 1292% inheritance not shown] (E) Log–log plot of boulder inheritance in ka versus gaussian age. (F) Log–log plot of inherited boulder age versus gaussian age. Vertical blue dashed line in all plots represents gLGM at 21 ka. Solid green line in plots (C and F) represent 1:1 ratio, while green dashed lines indicate percentages of age underestimation and inheritance, respectively. (For interpretation of the references to color in this figure legend, the reader is referred to the web version of this article.)

sourced from areas that are glaciated frequently; thus the amount of inherited  $^{10}\text{Be}$  will generally be less compared to material from areas that are glaciated less frequently (i.e. areas eroded by more extensive advances; Applegate et al., 2012).

The amounts of inherited  $^{10}\text{Be}$  produced during initial transport are generally small because glacial transport times are short. They can have a significant effect on very young deposits Little Ice Age and younger (LIA), but quickly become less important through time because  $^{10}\text{Be}$  concentrations on older landforms become comparably large.

Inheritance due to reworking can have a significant effect on old and young moraines. Reworking of landforms, that is, debris from glacial, alluvial fan, rock avalanche deposits can incorporate sediment with very large concentrations of inherited  $^{10}\text{Be}$ . Debris incorporated in this way are, theoretically, easy to identify as outliers though various statistical methods.

In this study we isolated 15 of 321  $^{10}\text{Be}$  ages from landforms older than the gLGM and 35 of 274 ages from landforms gLGM and younger in age (See plots in Appendix B and C for outliers). These outliers were plotted against the originating local glacial stage gaussian ages in both age and percent. Post-gLGM inheritance is three times as common (12.7% vs. 4.7%) and three times as significant (145% vs. 54%) on average compared to deposits older than the gLGM. This is graphically summarized in Fig. 13 (LGM plotted as blue dashed line), which shows the relative importance or percentage (Fig. 13D) of inherited  $^{10}\text{Be}$  decrease exponentially with age, in spite of the total amount of inheritance increasing (Fig. 13E). Overall, the amount of inheritance averages  $\sim 160\%$  until  $\leq 1.5$  ka where average inheritance increases toward 300% (Fig. 13F).

The decreasing influence of inheritance on  $^{10}\text{Be}$  ages is likely due to an age scaling effect where the *in situ* and reworking modes become more difficult to distinguish while the transport mode is small compared to the age. Small amounts of inheritance are difficult to isolate among old and scattered  $^{10}\text{Be}$  ages, thus the average amount of inherited  $^{10}\text{Be}$  is artificially increased while the occurrence is artificially decreased, that is, we cannot isolate 5 ka of inheritance on a landform older than 200 ka. Our method may be insensitive to inheritance of  $\sim 4\text{--}5\%$  at 10 ka and 100 ka old landforms, respectively (Fig. 13F). Again, more datasets need to be analyzed to confirm this. However, a small amount of inheritance on old boulders is likely compensated for by even minor erosion.

The reverse is true for post gLGM landforms where inheritance becomes increasingly important in spite of falling inherited  $^{10}\text{Be}$  concentrations. The proximity to the glacial source areas ensures frequent erosive periods, and would make inheritance due to both *in situ* and reworking pathways less common while increasing the importance of initial transport inheritance. However, *in situ* inheritance would still remain important on bedrock above headwalls with tor morphology. Tighter clustering of ages on young landforms enables smaller concentrations of inherited  $^{10}\text{Be}$ s can be isolated. For example, one hundred years of transport can be isolated on a LIA landform as it is above the  $\sim 4\%$  threshold of the gaussian separation method. Therefore, we suggest that the increase in inheritance at  $\leq 1.5$  ka may be due to exposure during transportation.

### 8.5.3. Summary

On average, of the 595 boulders analyzed, 8% have inheritance, 32% underestimate the age of the landform, and 60% have ages that are in-line with expected age distributions of a landform. Thus, to obtain three ages in a cluster, a minimum of 5 samples should be collected from moraines in the western Himalayan–Tibetan orogen. Age underestimation (192 boulders) is four times as common compared to inheritance (50 boulders); their significance (%) is comparable for landforms pre-gLGM in age. Envelopes are graphically expressed in Fig. 13C and F. These show that the degree of inheritance can easily

range between 0 and 300% on post-gLGM landforms whereas under exposure is always limited to 100% or less on all timescales. Trend lines express average inheritance of 160% (Fig. 13F) and age underestimation of  $\sim 45\%$  (Fig. 13C) across the entire time-scale.

Our gaussian isolation method identified exposure ages that are too old and too young in a pattern that is both theoretically expected, explainable, and in line with previous research (Barrows et al., 2007; Applegate et al., 2008, 2010; Chevalier et al., 2011; Heyman et al., 2011). Moreover, the degree with which gaussian separation can distinguish outliers (3–6%) is in line with age uncertainties (Fig. 13C and F). To our knowledge, the sensitivity of other methods has not been estimated.

## 9. Conclusions

Five local glacial stages are defined for the Ladakh Range, these include the Ladakh-4 glacial stage at  $81 \pm 20$  ka, the Ladakh-3 glacial stage between  $\sim 22$  and 81 ka, the Ladakh-2 glacial stage at  $22 \pm 3$  ka, Ladakh-1 glacial stage at  $\sim 2\text{--}22$  ka, and the Ladakh Cirque glacial stage at  $1.8 \pm 0.4$  ka. In addition, three local glacial stages are defined in the Pangong Range, which include the Pangong-2 glacial stage at  $85 \pm 15$  ka, the Pangong-1 glacial stage at  $40 \pm 3$  ka and the Pangong Cirque glacial stage at  $0.4 \pm 0.3$  ka.

We combined our new ages with published data for semi-arid regions across the Transhimalaya, Pamir, and Tian Shan towards the western end of the Himalayan–Tibetan orogen to develop a regional framework for glaciation. We define nineteen regional glacial stages, which we call semi-arid western Himalayan–Tibetan stages (SWHTS). Variation in spatial distribution of glaciation between regional stages due is likely driven by individual glacier sensitivity to temperature or precipitation.

SWHTS older than gLGM are broadly correlated with the MIS 9, 7, 6, 5E, 5A, 5A-, 4, 3, and 2. In addition, SWHTS gLGM and younger likely correlate with the Oldest Dryas, Older Dryas [tentative], Younger Dryas, Roman humid period, and the Little Ice Age. Termination of SWHTS 4, 3, 2F, and 2C correlate with Heinrich events 6, 5, 3, and 1, respectively. However, the linkage between Himalayan glaciation and Heinrich events remains unclear.

Of the 595 boulders analyzed, 8% have inheritance, 32% underestimate the age of the landform, and 60% have ages that are in-line with expected age distributions of a landform. Statistical analysis of outliers shows that the relative importance and occurrence of inherited  $^{10}\text{Be}$  decreases with age in spite of the total amount of isolated inheritance increasing. In contrast, the percentages of age underestimation clearly show no relationship with landform age (i.e. affects old and young landforms equally). Age underestimation (192 boulders) is four times as common compared to inheritance (50 boulders); however the relative importance of inheritance can reach three times the influence of exhumation on post-gLGM landform ages.

Our study provides the first regional chronology and climatic correlations for Himalayan–Tibetan glaciation. More extensive advances occur due to the influence of monsoons but the dominance of climatic systems changes with timescale; 30–146 ka glaciation is monsoon controlled while 21 ka to contemporary glaciation is generally controlled by the westerlies. We suggest that the frequent ( $2.2 \pm 0.7$  ka periodicity) post-gLGM glacial sediments are missing from the older pre-gLGM portion of glacial sequences ( $35 \pm 25$  ka periodicity) due to extensive subsequent monsoon driven glaciation destroying the less extensive westerly driven glacial debris.

This framework can be utilized in future glacial geologic, paleoenvironmental, ice volume modeling, and landscape evolution studies. This has significant ramifications not only for climate modeling and glacial land cover estimates, but also for erosion based studies. For example, which has the greatest effect on the shaping and incision of topography: more rapid and less extensive variations

in glaciation on short timescales driven by the mid-latitude westerlies, or less frequent more extensive advances driven by the monsoon? Thus, our framework can form the foundation for new questions on how we obtain erosion estimates and what timescales are appropriate to compare an average ELA to topography.

## Acknowledgments

We thank Dr. Madhav Murari and Dr. Patrick Applegate for help and discussion on gaussian separation, Susan Ma and PRIME Laboratory for help with cosmogenic dating, reviewers Dr. Jacob Heyman and Dr. Yeong Bae Seong for excellent reviews that helped to improve this manuscript and Dr. Neil Glasser for being a patient editor. JD thanks the University of Cincinnati Geochronology Laboratories; Sigma Xi, the American Alpine Club for funding this project. JD also thanks Kara the hammer for years of faithful service collecting 100's of cosmogenic and dozens of thermochronology samples before finally making the ultimate sacrifice to scientific progress. LAO and MWC thank the University of Cincinnati for funding their field cost.

## Appendix A. Supplementary data

Supplementary data related to this article can be found at <http://dx.doi.org/10.1016/j.quascirev.2013.07.025>.

## References

- Abramowski, U., Bergau, A., Seebach, D., Zech, R., Glaser, B., Sosin, P., Kubik, P.W., Zech, W., 2006. Pleistocene glaciations of Central Asia: results from  $^{10}\text{Be}$  surface exposure ages of erratic boulders from the Pamir (Tajikistan) and the Alay-Turkestan range (Kyrgyzstan). *Quaternary Science Reviews* 25, 1080–1096.
- Applegate, P.J., Lowell, T.V., Alley, R.B., 2008. Comment on "Absence of cooling in New Zealand and the adjacent ocean during the Younger Dryas Chronozone". *Science* 320, 746.
- Applegate, P.J., Urban, N.M., Laabs, B.J.C., Keller, K., Alley, R.B., 2010. Modeling the statistical distributions of cosmogenic exposure dates from moraines. *Geoscientific Model Development* 3, 293–307.
- Applegate, P.J., Urban, N.M., Keller, K., Lowell, T.V., Laabs, B.J.C., Kelly, M.A., Alley, R.B., 2012. Improved moraine age interpretations through explicit matching of geomorphic process models to cosmogenic nuclide measurements from single landforms. *Quaternary Research* 77, 293–304.
- Balco, G., Stone, J.O., Lifton, N.A., Dunai, T.J., 2008. A complete and easily accessible means of calculating surface exposure ages or erosion rates from  $^{10}\text{Be}$  and  $^{26}\text{Al}$  measurements. *Quaternary Geochronology* 8, 174–195.
- Barrows, T.T., Lehman, S.J., Fifield, L.K., Deckker, P.D., 2007. Absence of cooling in New Zealand and the adjacent ocean during the Younger Dryas Chronozone. *Science* 318, 86–89.
- Benn, D.I., Owen, L.A., 1998. The role of the Indian summer monsoon and the mid-latitude westerlies in Himalayan glaciation: review and speculative discussion. *Journal of the Geological Society, London* 155, 353–363.
- Bookhagen, B., Thiede, R.C., Strecker, M.R., 2005. Late Quaternary intensified monsoon phases control landscape evolution in the northwest Himalaya. *Geology* 33, 149–152.
- Bookhagen, B., Burbank, D.W., 2006. Topography, relief, and TRMM-derived rainfall variations along the Himalaya. *Geophysical Research Letters* 33, L08405. <http://dx.doi.org/10.1029/2006GL026037>.
- Bookhagen, B., 2013. High resolution spatiotemporal distribution of rainfall seasonality and extreme events based on a 12-year TRMM time series (submitted for publication) <http://www.geog.ucsb.edu/~bodo/TRMM/>.
- Briner, J.P., Kaufman, D.S., Manley, W.F., Finkel, R.C., Caffee, M.W., 2005. Cosmogenic exposure dating of late Pleistocene moraine stabilization in Alaska. *Geological Society of America Bulletin* 117, 1108–1120.
- Briner, J.P., Young, N.E., Goehring, B.M., Schaefer, J.M., 2012. Constraining Holocene  $^{10}\text{Be}$  production rates in Greenland. *Journal of Quaternary Science* 27, 2–6.
- Brown, E.T., Bendick, R., Bourles, D.L., Gaur, V., Molnar, P., Raisbeck, G.M., Yiou, F., 2002. Slip rates of the Karakoram fault, Ladakh, India, determined using cosmic ray exposure dating of debris flows and moraines. *Journal of Geophysical Research* 107 (B9), 7-1–7-8, 2192.
- Brown, E.T., Bendick, R., Bourlés, D.L., Gaur, V., Molnar, P., Raisbeck, G.M., Yiou, F., 2003. Early Holocene climate recorded in geomorphological features in Western Tibet. *Palaeogeography, Palaeoclimatology, Palaeoecology* 199, 141–151.
- Brozović, N., Burbank, D.W., Meigs, A.J., 1997. Climatic limits on landscape development in the northwestern Himalaya. *Science* 276, 571–574.
- Burbank, D.W., Fort, M.B., 1985. Bedrock control on glacial limits: examples from the Ladakh and Zaskar Ranges, north-western Himalaya, India. *Journal of Glaciology* 31, 143–149.
- Chevalier, M.-L., Hilley, G., Tapponnier, P., Van Der Woerd, J., Liu-Zeng, J., Finkel, R.C., Ryerson, F.J., Li Haibing, L., Liu, X., 2011. Constraints on the late Quaternary glaciations in Tibet from cosmogenic exposure ages of moraine surfaces. *Quaternary Science Reviews* 30, 528–554.
- CGIAR-CSI, 2007. The CGIAR Consortium for Spatial Information. <http://srtm.csi.cgiar.org/SELECTION/inputCoord.asp>. Accessed on August 2012.
- Cronin, V.S., Johnson, W.P., Johnson, N.M., Johnson, G.D., 1989. Chronostratigraphy of the upper Cenozoic Bunthang sequence and possible mechanisms controlling base level in Skardu intermontane basin, Karakoram, Himalaya, Pakistan. *Geological Society of America Special Paper* 232, 295–309.
- Damm, B., 2006. Late Quaternary glacier advances in the upper catchment area of the Indus River (Ladakh and Western Tibet). *Quaternary International* 154–155, 87–89.
- Demske, D., Tarasov, P.E., Wünnemann, B., Riedel, F., 2009. Late glacial and Holocene vegetation, Indian monsoon and westerly circulation in the Trans-Himalaya recorded in the lacustrine pollen sequence from Tso Kar, Ladakh, NW India. *Palaeogeography, Palaeoclimatology, Palaeoecology* 279, 172–185.
- Dewey, J.F., Cande, S., Pitman, W.C., 1989. Tectonic evolution of the India–Eurasia collision zone. *Ecolage Helvetiae* 82, 717–734.
- Dortch, J., Owen, L.A., Haneberg, W.C., Caffee, M.W., Dietsch, C., Kamp, U., 2009. Nature and timing of large-landslides in northern India. *Quaternary Science Reviews* 28, 1037–1056.
- Dortch, J.M., Owen, L.A., Caffee, M.W., 2010a. Quaternary glaciation in the Nubra and Shyok valley confluence, northernmost Ladakh, India. *Quaternary Research* 74, 132–144.
- Dortch, J., Owen, L.A., Caffee, M.W., Brease, P., 2010b. Late Quaternary glaciation and equilibrium line altitude variations of the McKinley River region, central Alaska Range. *Boreas* 39, 233–246.
- Dortch, J.M., Owen, L.A., Schoenbohm, L.M., Caffee, M.W., 2011a. Asymmetrical erosion and morphological development of the Ladakh Range, northern India. *Geomorphology* 135, 167–180.
- Dortch, J.M., Owen, L.A., Caffee, M.W., Kamp, U., 2011b. Catastrophic partial drainage of Pangong Tso, northern India and Tibet. *Geomorphology* 125, 109–121.
- Douglass, D.C., Singer, B.S., Kaplan, M.R., Mickelson, D.M., Caffee, M.W., 2006. Cosmogenic nuclide surface exposure dating of boulders on last-glacial and late-glacial moraines, Lago Buenos Aries, Argentina: interpretive strategies and paleoclimatic implications. *Quaternary Geochronology* 1, 43–58.
- Dunlap, W.J., Weinberg, R.F., Searle, M.P., 1998. Karakoram fault zone rocks cool in two phases. *Journal of the Geological Society, London* 155, 903–912.
- Eyles, N., Boyce, J.I., Barendregt, R.W., 1999. Hummocky moraine: sedimentary record of stagnant Laurentide Ice Sheet lobes resting on soft beds. *Sedimentary Geology* 123, 163–174.
- Fort, M., 1983. Geomorphological observations in the Ladakh area (Himalayas): Quaternary evolution and present dynamics. In: Gupta, V.J. (Ed.), *Stratigraphy and Structure of Kashmir and Ladakh Himalaya*. Hindustan Publishing Corporation, New Delhi, India, pp. 39–58.
- Gasse, F., Fontes, J.C., Van Campo, E., Wei, K., 1996. Holocene environmental changes in Bangong Co basin (Western Tibet). Part 4: discussion and conclusions. *Palaeogeography, Palaeoclimatology, Palaeoecology* 120, 79–92.
- Goehring, B.M., Lohne, Ø.S., Mangerud, J., Svendsen, J.I., Gyllencreutz, R., Schaefer, J., Finkel, R., 2012. Late glacial and Holocene  $^{10}\text{Be}$  production rates for western Norway. *Journal of Quaternary Science* 27, 89–96.
- Grove, J.M., 2004. *Little Ice Ages. Ancient and Modern*, second ed., vol. 1 and 2. Routledge, London, New York, pp. 1–178.
- Hambrey, M.J., Huddart, D., Bennett, M.R., Glasser, N.F., 1997. Genesis of 'hummocky moraines' by thrusting in glacier ice: evidence from Svalbard and Britain. *Journal of the Geological Society, London* 154, 623–632.
- Hedrick, K.A., Seong, Y.B., Owen, L.A., Caffee, M.C., Dietsch, C., 2011. Towards defining the transition in style and timing of Quaternary glaciation between the monsoon-influenced Greater Himalaya and the semi-arid Transhimalaya of Northern India. *Quaternary International* 236, 21–33.
- Hemming, S.R., 2004. Heinrich events: massive late Pleistocene detritus layers of the North Atlantic and their global climate imprint. *Reviews of Geophysics* 42, RG1005. <http://dx.doi.org/10.1029/2003RG000128>.
- Heyman, J., Stroeven, A., Harbor, J., Caffee, M.W., 2011. Too young or too old: evaluating 884 cosmogenic exposure dating based on an analysis of compiled boulder exposure 885 ages. *Earth and Planetary Science Letters* 302, 71–80.
- Hobley, D.E.J., Sinclair, H.D., Cowie, P.A., 2010. Process, rates, and time scales of fluvial response in an ancient postglacial landscape of the northwestern Indian Himalaya. *Geological Society of America Bulletin* 122, 1569–1584.
- Hobley, D.E.J., Sinclair, H.D., Mudd, S.M., 2012. Reconstruction of the hydrology of a major storm event from its geomorphic signature: the Ladakh cloudburst, 6 August 2010. *Geology* 40, 483–486.
- Hughes, P.D., Gibbard, P.L., Woodward, J.C., 2005. Quaternary glacial records in mountain regions: a formal stratigraphical approach. *Episodes* 28, 85–92.
- Ivy-Ochs, S., Kerschner, H., Schlüchter, C., 2007. Cosmogenic nuclides and the dating of lateglacial and Early Holocene glacial variations: the Alpine perspective. *Quaternary International* 164–165, 53–63.
- Ivy-Ochs, S., Kerschner, H., Reuther, A., Preusser, F., Heine, K., Maisch, M., Kubik, P.W., Schlüchter, C., 2008. Chronology of the last glacial cycle in the European Alps. *Journal of Quaternary Science* 23, 559–573.

- Jamieson, S.S.R., Sinclair, H.D., Kirstein, L.A., Purves, R.S., 2004. Tectonic forcing of longitudinal valleys in the Himalaya: morphological analysis of the Ladakh Batholith, North India. *Geomorphology* 58, 49–65.
- Johnson, M.W.R., 2002. Shortening budgets and the role of continental subduction during the India–Asia collision. *Earth Science Reviews* 59, 101–123.
- Kirstein, L.A., Foeken, J.P.T., van der Beek, P., Stuart, F.M., Phillips, R.J., 2009. Cenozoic unroofing history of the Ladakh batholith, western Himalaya, constrained by thermochronology and numerical modeling. *Journal of the Geological Society, London* 166, 667–678.
- Kirstein, L.A., 2011. Thermal evolution and exhumation of the Ladakh batholith, northwest Himalaya, India. *Tectonophysics* 503, 222–233.
- Kirstein, L.A., Sinclair, H., Stuart, F.M., Dobson, K., 2006. Rapid early Miocene exhumation of the Ladakh batholiths, western Himalaya. *Geology* 34, 1049–1052.
- Kohl, C.P., Nishiizumi, K., 1992. Chemical isolation of quartz for measurement of in-situ produced cosmogenic nuclides. *Geochimica et Cosmochimica Acta* 56, 3583–3587.
- Koppes, M., Gillespie, A.R., Burke, R.M., Thompson, S.C., Stone, J., 2008. Late Quaternary glaciation in the Kyrgyz Tien Shan. *Quaternary Science Reviews* 27, 846–866.
- Korup, O., Montgomery, D.R., 2008. Tibetan plateau river incision inhibited by glacial stabilization of the Tsangpo gorge. *Nature* 455, 786–789.
- Kumar, R., Lal, N., Singh, S., Jain, A.K., 2007. Cooling and exhumation of the Trans-Himalayan Ladakh batholith as constrained by fission track apatite and zircon ages. *Current Science* 92, 490–496.
- Lal, D., 1991. Cosmic ray labeling of erosion surfaces: in situ nuclide production rates and erosion models. *Earth and Planetary Science Letters* 104, 429–439.
- Lee, S.U., Seong, Y.B., Owen, L.A., Murari, M.K., Lim, H.S., Yoon, H.I., Yoo, K.C., 2013. Late Quaternary glaciation in the Nun-Kun massif, northwestern India. *Boreas*. <http://dx.doi.org/10.1111/bor.12022>.
- Lehmkuhl, F., Owen, L.A., 2005. Late Quaternary glaciation of Tibet and the bordering mountains: a review. *Boreas* 34, 87–100.
- Leuschner, D.C., Sirocko, F., 2003. Orbital insolation forcing of the Indian Monsoon—a motor for global climate changes? *Palaeogeography, Palaeoclimatology, Palaeoecology* 197, 83–95.
- Lifton, N.A., Bieber, J.W., Clem, J.M., Duldig, M.L., Evenson, P., Humble, J.E., Pyle, R., 2005. Addressing solar modulation and long-term uncertainties in scaling secondary cosmic rays for in situ cosmogenic nuclide applications. *Earth and Planetary Science Letters* 239, 140–161.
- Lisiecki, L.E., Raymo, M.E., 2005. A Pliocene–Pleistocene stack of 57 globally distributed benthic  $\delta^{18}\text{O}$  records. *Paleoceanography* 20. <http://dx.doi.org/10.1029/2004PA001071>.
- Miehe, G., Winiger, M., Bohner, J., Yili, Z., 2001. Climatic diagram map of high Asia. Purpose and concepts. *Erdkunde* 55, 94–97.
- Mix, A.C., Bard, E., Schneider, R., 2001. Environmental processes of the ice age: land, ocean, glaciers (EPiLOG). *Quaternary Science Reviews* 20, 627–657.
- Molnar, P., England, P., 1990. Late Cenozoic uplift of mountain ranges and global climatic change: chicken or egg? *Nature* 46, 29–34.
- North Greenland Ice Core Project members, 2004. High-resolution record of Northern Hemisphere climate extending into the last interglacial period. *Nature* 431, 147–151.
- Norton, K.P., Abbühl, L.M., Schlunegger, F., 2010. Glacial conditioning as an erosional driving force in the Central Alps. *Geology* 38, 655–658.
- Owen, L.A., 2009. Latest Pleistocene and Holocene glacier fluctuations in the Himalaya and Tibet. *Quaternary Science Reviews* 28, 2150–2164.
- Owen, L.A., Derbyshire, E., Fort, M., 1998. The Quaternary glacial history of the Himalaya. *Quaternary Proceedings* 6, 91–120.
- Owen, L.A., Dortch, J.M., 2013. Nature and timing of Quaternary glaciation in the Himalayan–Tibetan orogen: a review. *Quaternary Science Reviews* (submitted for publication).
- Owen, L.A., Finkel, R.C., Barnard, P.L., Ma, H., Asahi, K., Caffee, M.W., Derbyshire, E., 2005. Climatic and topographic controls on the style and timing of Late Quaternary glaciation throughout Tibet and the Himalaya defined by  $^{10}\text{Be}$  cosmogenic radionuclide surface exposure dating. *Quaternary Science Reviews* 24, 1391–1411.
- Owen, L.A., Gualtieri, L., Finkel, R.C., Caffee, M.W., Benn, D.J., Sharma, M.C., 2001. Cosmogenic radionuclide dating of glacial landforms in the Lahul Himalaya, Northern India: defining the timing of Late Quaternary glaciation. *Journal of Quaternary Science* 16, 555–563.
- Owen, L.A., Finkel, R.C., Caffee, M.W., Gualtieri, L., 2002. Timing of multiple glaciations during the Late Quaternary in the Hunza Valley, Karakoram Mountains, Northern Pakistan: defined by cosmogenic radionuclide dating of moraines. *Geological Society of America Bulletin* 114, 593–604.
- Owen, L.A., Finkel, R.C., Ma, H., Spencer, J.Q., Derbyshire, E., Barnard, P.L., Caffee, M.W., 2003. Timing and style of Late Quaternary glaciations in NE Tibet. *Geological Society of America Bulletin* 11, 1356–1364.
- Owen, L.A., Caffee, M., Bovard, K., Finkel, R.C., Sharma, M., 2006. Terrestrial cosmogenic surface exposure dating of the oldest glacial successions in the Himalayan orogen. *Geological Society of America Bulletin* 118, 383–392.
- Owen, L.A., Caffee, M.W., Finkel, R.C., Seong, B.Y., 2008. Quaternary glaciations of the Himalayan–Tibetan orogen. *Journal of Quaternary Science* 23, 513–532.
- Owen, L.A., Frankel, K.L., Knott, J.R., Reynhout, S., Finkel, R.C., Dolan, J.F., Lee, J., 2011. Beryllium-10 terrestrial cosmogenic nuclide surface exposure dating of Quaternary landforms in Death Valley. *Geomorphology* 125, 541–557.
- Owen, L.A., Chen, J., Hedrick, K.A., Caffee, M.W., Robinson, A., Schoenbohm, L.M., Zhao, Y., Li, W., Imrecke, D., Liu, J., 2012. Quaternary glaciation of the Tashkurgan Valley, Southeast Pamir. *Quaternary Science Reviews* 47, 56–72.
- Phillips, W.M., Sloan, V.F., Shroder Jr., J.F., Sharma, P., Clarke, M.L., Rendell, H.M., 2000. Asynchronous glaciation at Nanga Parbat, northwestern Himalaya Mountains, Pakistan. *Geology* 28, 431–434.
- Putkonen, J., Swanson, T., 2003. Accuracy of cosmogenic ages for moraines. *Quaternary Research* 59, 255–261.
- Putkonen, J., O’Neal, M.A., 2006. Degradation of unconsolidated Quaternary landforms in the western North America. *Geomorphology* 75, 408–419.
- Reynhout, S.A., Dietsch, C., Dortch, J.M., Owen, L.A., Caffee, M.W., 2013. Very slow erosion and topographic evolution of the southern Ladakh Range, India. *Earth Surface Processes and Landforms* (submitted for publication).
- Richards, B.W.M., Owen, L.A., Rhodes, E.J., 2000a. Timing of Late Quaternary glaciations in the Himalayas of northern Pakistan. *Journal of Quaternary Science* 15, 283–297.
- Richards, B.W.M., Benn, D., Owen, L.A., Rhodes, E.J., Spencer, J.Q., 2000b. Timing of Late Quaternary glaciations south of Mount Everest in the Khumbu Himal, Nepal. *Geological Society of America Bulletin* 112, 1621–1632.
- Röhlinger, I., Zech, R., Abramowski, U., Sosin, P., Aldahan, A., Kubik, P.W., Zöller, L., Zech, W., 2012. The late Pleistocene glaciation in the Boghchigir Valleys (Pamir, Tajikistan) based on  $^{10}\text{Be}$  surface exposure dating. *Quaternary Research* 78, 590–597.
- Seong, Y.B., Owen, L.A., Bishop, M.P., Bush, A., Clendon, P., Copland, P., Finkel, R.C., Kamp, U., Shroder, J.F., 2007. Quaternary glacial history of the Central Karakoram. *Quaternary Science Reviews* 26, 3384–3405.
- Seong, Y.B., Bishop, M.P., Bush, A., Clendon, P., Copland, P., Finkel, R., Kamp, U., Owen, L.A., Shroder, J.F., 2009a. Landforms and landscape evolution in the Skardu, Shigar and Braldu Valleys, Central Karakoram. *Geomorphology* 103, 251–267.
- Seong, Y.B., Owen, L.A., Yi, C., Finkel, R.C., Schoenbohm, L., 2009b. Geomorphology of anomalously high glaciated mountains at the northwestern end of Tibet: Muztag Ata and Kongur Shan. *Geomorphology* 103, 227–250.
- Seong, Y.B., Owen, L.A., Yi, C., Finkel, R.C., 2009c. Quaternary glaciation of Muztag Ata and Kongur Shan: evidence for glacier response to rapid climate changes throughout the Late Glacial and Holocene in westernmost Tibet. *Geological Society of America Bulletin* 121, 348–365.
- Seong, Y.B., Owen, L.A., Caffee, M.W., Kamp, U., Bishop, M.P., Bush, A., Copland, L., Shroder, J.F., 2009d. Rates of basin-wide rockwall retreat in the K2 region of the Central Karakoram defined by terrestrial cosmogenic nuclide  $^{10}\text{Be}$ . *Geomorphology* 107, 254–262.
- Stone, J.O., 2000. Air pressure and cosmogenic isotope production. *Journal of Geophysical Research* 105, 23753–23759.
- Taylor, P.J., Mitchell, W.A., 2000. Late Quaternary glacial history of the Zaskar Range, North-west Indian Himalaya. *Quaternary International* 65/66, 81–100.
- Thompson, L.G., Yao, T., Davis, M.E., Hendersson, K.A., Mosley-Thompson, E., Lin, P.-N., Beer, J., Synal, H.A., Cole-Dai, J., Bolzan, J.F., 1997. Tropical climate instability: the Last Glacial Cycle from a Qinghai–Tibetan ice core. *Science* 276, 1821–1825.
- USGS EarthExplorer, 2011. Landsat ETM+ Data from U.S. Geological Survey Department of the Interior/USGS U.S. Geological Survey. Last accessed 2011.
- Willett, S.D., 2010. Erosion on a line. *Tectonophysics* 484, 168–180.
- Wang, Y.J., Cheng, H., Edwards, R.L., An, Z.S., Wu, J.Y., Shen, C.-C., Dorale, J.A., 2001. A High-Resolution Absolute-Dated Late Pleistocene Monsoon Record from Hulu Cave, China. *Science* 294, 2345–2348.
- Wang, Y., Cheng, H., Edwards, R.L., Kong, X., Shao, X., Chen, S., Wu, J., Jiang, X., Wang, X., An, Z., 2008. Millennial- and orbital-scale changes in the East Asian monsoon over the past 224,000 years. *Nature*, 1090–1093.
- Zech, R., Abramowski, U., Glaser, B., Sosin, P., Kubik, P.W., Zech, W., 2005a. Late Quaternary glacial and climate history of the Pamir Mountains derived from cosmogenic  $^{10}\text{Be}$  exposure ages. *Quaternary Research* 64, 212–220.
- Zech, W., Glaser, B., Sosin, P., Kubik, P.W., Zech, W., 2005b. Evidence for long-lasting landform surface instability on hummocky moraines in the Pamir Mountains (Tajikistan) from  $^{10}\text{Be}$  surface exposure dating. *Earth and Planetary Science Letters* 237, 453–461.
- Zech, R., 2012. A Late Pleistocene glacial chronology from the Kitschi-Kurumdu Valley, Tien Shan (Kyrgyzstan), based on  $^{10}\text{Be}$  surface exposure dating. *Quaternary Research* 77, 281–288.
- Zech, R., Röhlinger, I., Sosin, P., Kabgov, H., Merchel, S., Akhmadaliev, S., Zech, W., 2013. Late Pleistocene glaciations in the Gissar Range, Tajikistan, based on  $^{10}\text{Be}$  surface exposure dating. *Palaeogeography, Palaeoclimatology, Palaeoecology* 369, 253–261.
- Zeitler, P.K., Meltzer, A.S., Koons, P.O., Craw, D., Hallet, B., Chamberlain, C.P., Kidd, W.S.F., Park, S.K., Seiber, L., Bishop, M., Shroder, J.F., 2001. Erosion, Himalayan geodynamics and the geomorphology of metamorphism. *GSA Today* 11, 4–8.